

See discussions, stats, and author profiles for this publication at: <https://www.researchgate.net/publication/24305609>

# Pyrrolidinium Ionic Liquid Crystals with Pendant Mesogenic Groups

ARTICLE *in* LANGMUIR · MAY 2009

Impact Factor: 4.46 · DOI: 10.1021/la900048h · Source: PubMed

---

CITATIONS

35

READS

40

## 8 AUTHORS, INCLUDING:



[Peter Nockemann](#)

Queen's University Belfast

168 PUBLICATIONS 3,379 CITATIONS

[SEE PROFILE](#)



[Kristof Van Hecke](#)

Ghent University

179 PUBLICATIONS 2,803 CITATIONS

[SEE PROFILE](#)



[Thomas Cardinaels](#)

Belgian Nuclear Research Centre

32 PUBLICATIONS 743 CITATIONS

[SEE PROFILE](#)

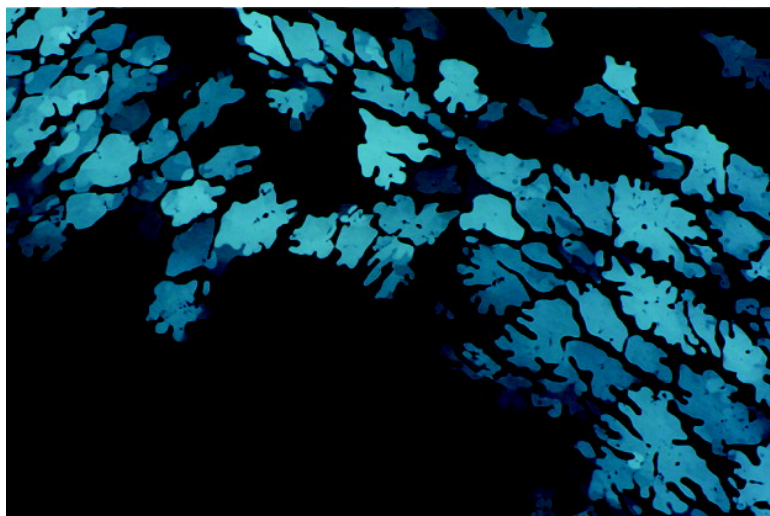
Article

## Pyrrolidinium Ionic Liquid Crystals with Pendant Mesogenic Groups

Karel Goossens, Kathleen Lava, Peter Nockemann, Kristof Van Hecke,  
Luc Van Meervelt, Phil Pattison, Koen Binnemans, and Thomas Cardinaels

*Langmuir*, 2009, 25 (10), 5881-5897 • DOI: 10.1021/la900048h • Publication Date (Web): 20 April 2009

Downloaded from <http://pubs.acs.org> on May 12, 2009



### More About This Article

Additional resources and features associated with this article are available within the HTML version:

- Supporting Information
- Access to high resolution figures
- Links to articles and content related to this article
- Copyright permission to reproduce figures and/or text from this article

[View the Full Text HTML](#)



**ACS Publications**  
High quality. High impact.

Langmuir is published by the American Chemical Society. 1155 Sixteenth Street N.W., Washington, DC 20036

## Pyrrolidinium Ionic Liquid Crystals with Pendant Mesogenic Groups

Karel Goossens,<sup>†</sup> Kathleen Lava,<sup>†</sup> Peter Nockemann,<sup>†</sup> Kristof Van Hecke,<sup>†</sup> Luc Van Meervelt,<sup>†</sup> Phil Pattison,<sup>‡</sup> Koen Binnemans,<sup>†</sup> and Thomas Cardinaels\*,<sup>†</sup>

<sup>†</sup>Department of Chemistry, Katholieke Universiteit Leuven, Celestijnenlaan 200F, P.O. Box 2404, B-3001 Leuven, Belgium, and <sup>‡</sup>Swiss-Norwegian Beamline (SNBL) at the European Synchrotron Radiation Facility (ESRF), Rue Jules Horowitz, F-38043 Grenoble, France

Received November 17, 2008. Revised Manuscript Received March 20, 2009

New ionic liquid crystals (including ionic metallomesogens) based on the pyrrolidinium core are presented. *N*-Methylpyrrolidine was quaternized with different mesogenic groups connected to a flexible,  $\omega$ -bromosubstituted alkyl spacer. The length of the flexible alkyl spacer between the cationic head group and the rigid mesogenic group was varied. The substituted pyrrolidinium cations were combined with bromide, bis(trifluoromethylsulfonyl)imide, tetrakis (2-thienoyl trifluoroacetato)europeate(III), and tetrabromouranyl anions. The influence of the type of mesogenic unit, the lengths of the flexible spacer and terminal alkyl chain, the size of the mesogenic group, and the type of anion on the thermotropic mesomorphic behavior was investigated. Furthermore, the phase behavior was thoroughly compared with the previously reported mesomorphism of *N*-alkyl-*N*-methylpyrrolidinium salts. Low-ordered smectic A phases of the de Vries type, smectic C phases, higher-ordered smectic F/I phases, as well as crystal smectic phases (E and G, J, H, or K) were observed and investigated by polarizing optical microscopy, differential scanning calorimetry, and powder X-ray diffraction.

### Introduction

The interest in ionic liquid crystals has increased significantly in recent years, partly due to the growing research activities in the field of ionic liquids.<sup>1</sup> The ionic nature of these compounds can lead to a larger mesophase stability range in comparison to nonionic analogues,<sup>2</sup> and allows one to obtain uncommon mesophases such as the crystal smectic T phase<sup>3–5</sup> or the nematic columnar phase.<sup>6</sup> It has been shown that aligned samples of ionic liquid crystals can exhibit a pronounced anisotropic ion conduction,<sup>7</sup> and that ionic metallomesogens can be used as an anisotropic reaction medium for the shape-selective synthesis of nanoparticles.<sup>8,9</sup> Different cationic cores have been investigated,

among them imidazolium,<sup>10–12</sup> pyridinium,<sup>10,13–17</sup> quaternary ammonium,<sup>3,4,18</sup> and quaternary phosphonium cores.<sup>19–22</sup> In general, the liquid-crystalline behavior of the ionic salts strongly depends on the nature of both the cation and the anion and on the length of the alkyl chain of the organic cation. Recently, we reported on the mesomorphic properties of thermotropic liquid-crystalline *N*-alkyl-*N*-methylpyrrolidinium compounds.<sup>5</sup> The pyrrolidinium core offers advantages for studies of the metal-centered luminescence of ionic metallomesogens, because it shows no inconvenient background fluorescence. Furthermore, as far as the thermal behavior is concerned, one can compare the well-known imidazolium-based liquid crystals and pyrrolidinium-based mesogens. Both cationic cores consist of a five-membered heterocyclic ring, but they differ in shape (the imidazolium ring is planar while the pyrrolidinium ring is not) and charge distribution (charge delocalization in the imidazolium ring in contrast to a positive point charge in the pyrrolidinium ring). It is well-known that halide salts with heteroaromatic cations show extensive nonclassical C–H $\cdots$ X hydrogen bonding.<sup>12,23–33</sup> Very recently,

- \*Corresponding author. E-mail: thomas.cardinaels@chem.kuleuven.be.  
(1) Binnemans, K. *Chem. Rev.* **2005**, *105*, 4148–4204.  
(2) Motoyanagi, J.; Fukushima, T.; Aida, T. *Chem. Commun.* **2005**, 101–103.  
(3) Alami, E.; Levy, H.; Zana, R.; Weber, P.; Skoulios, A. *Liq. Cryst.* **1993**, *13*, 201–212.  
(4) Arkas, M.; Tsiorvas, D.; Paleos, C. M.; Skoulios, A. *Chem.—Eur. J.* **1999**, *5*, 3202–3207.  
(5) Goossens, K.; Lava, K.; Nockemann, P.; Van Hecke, K.; Van Meervelt, L.; Driesen, K.; Görller-Walrand, C.; Binnemans, K.; Cardinaels, T. *Chem.—Eur. J.* **2009**, *15*, 656–674.  
(6) Artzner, F.; Veber, M.; Clerc, M.; Levelut, A. M. *Liq. Cryst.* **1997**, *23*, 27–33.  
(7) Yoshio, M.; Mukai, T.; Ohno, H.; Kato, T. *J. Am. Chem. Soc.* **2004**, *126*, 994–995.  
(8) Taubert, A. *Angew. Chem., Int. Ed.* **2004**, *43*, 5380–5382.  
(9) Dobbs, W.; Suisse, J. M.; Douce, L.; Welter, R. *Angew. Chem., Int. Ed.* **2006**, *45*, 4179–4182.  
(10) Bowlas, C. J.; Bruce, D. W.; Seddon, K. R. *Chem. Commun.* **1996**, 1625–1626.  
(11) Bradley, A. E.; Hardacre, C.; Holbrey, J. D.; Johnston, S.; McMath, S. E. J.; Nieuwenhuizen, M. *Chem. Mater.* **2002**, *14*, 629–635.  
(12) Goossens, K.; Nockemann, P.; Driesen, K.; Goderis, B.; Görller-Walrand, C.; Van Hecke, K.; Van Meervelt, L.; Pouzet, E.; Binnemans, K.; Cardinaels, T. *Chem. Mater.* **2008**, *20*, 157–168.  
(13) Knight, G. A.; Shaw, B. D. *J. Chem. Soc.* **1938**, 682–683.  
(14) Navarro-Rodríguez, D.; Frère, Y.; Gramain, P.; Guillon, D.; Skoulios, A. *Liq. Cryst.* **1991**, *9*, 321–335.  
(15) Cruz, C.; Heinrich, B.; Ribeiro, A. C.; Bruce, D. W.; Guillon, D. *Liq. Cryst.* **2000**, *27*, 1625–1631.  
(16) Cui, L.; Sapagovas, V.; Lattermann, G. *Liq. Cryst.* **2002**, *29*, 1121–1132.  
(17) Neve, F.; Francescangeli, O.; Crispini, A.; Charmant, J. *Chem. Mater.* **2001**, *13*, 2032–2041.  
(18) Lu, L.; Sharma, N.; Gowda, G. A. N.; Khetrapal, C. L.; Weiss, R. G. *Liq. Cryst.* **1997**, *22*, 23–28.  
(19) Abdallah, D. J.; Robertson, A.; Hsu, H. F.; Weiss, R. G. *J. Am. Chem. Soc.* **2000**, *122*, 3053–3062.

- (20) Chen, H.; Kwait, D. C.; Gonon, Z. S.; Weslowski, B. T.; Abdallah, D. J.; Weiss, R. G. *Chem. Mater.* **2002**, *14*, 4063–4072.  
(21) Ma, K. F.; Somashekhar, B. S.; Gowda, G. A. N.; Khetrapal, C. L.; Weiss, R. G. *Langmuir* **2008**, *24*, 2746–2758.  
(22) Ma, K.; Shahkhatuni, A. A.; Somashekhar, B. S.; Gowda, G. A. N.; Tong, Y.; Khetrapal, C. L.; Weiss, R. G. *Langmuir* **2008**, *24*, 9843–9854.  
(23) Abdul-Sada, A. K.; Greenway, A. M.; Hitchcock, P. B.; Mohammed, T. J.; Seddon, K. R.; Zora, J. A. *J. Chem. Soc., Chem. Commun.* **1986**, 1753–1754.  
(24) Abdul-Sada, A. K.; Al-Juaid, S.; Greenway, A. M.; Hitchcock, P. B.; Howells, M. J.; Seddon, K. R.; Welton, T. *Struct. Chem.* **1990**, *1*, 391–394.  
(25) Hitchcock, P. B.; Seddon, K. R.; Welton, T. *J. Chem. Soc., Dalton Trans.* **1993**, 2639–2643.  
(26) Aakeröy, C. B.; Seddon, K. R. *Z. Naturforsch., B: Chem. Sci.* **1993**, *48*, 1023–1025.  
(27) Elaiwi, A.; Hitchcock, P. B.; Seddon, K. R.; Srinivasan, N.; Tan, Y. M.; Welton, T.; Zora, J. A. *J. Chem. Soc., Dalton Trans.* **1995**, 3467–3472.  
(28) Steiner, T. *Acta Crystallogr., Sect. B: Struct. Sci.* **1998**, *54*, 456–463.  
(29) Aakeröy, C. B.; Evans, T. A.; Seddon, K. R.; Palinko, I. *New J. Chem.* **1999**, *23*, 145–152.  
(30) Steiner, T. *Angew. Chem., Int. Ed.* **2002**, *41*, 48–76.  
(31) Desiraju, G. R. *Acc. Chem. Res.* **2002**, *35*, 565–573.  
(32) van den Berg, J. A.; Seddon, K. R. *Crys. Growth Des.* **2003**, *3*, 643–661.  
(33) Berg, R. W.; Deetlefs, M.; Seddon, K. R.; Shim, I.; Thompson, J. M. *J. Phys. Chem. B* **2005**, *109*, 19018–19025.

it was found that pyrrolidinium chloride salts such as *N*-methyl-*N*-propylpyrrolidinium chloride also form networks of weak C—H···Cl<sup>−</sup> hydrogen bonds in the crystalline solid state (H···Cl<sup>−</sup> distances between 2.72 and 2.87 Å).<sup>34</sup> Very weak C—H···I<sup>−</sup> interactions were also found in crystals of *N*,*N*-dimethylpyrrolidinium iodide at 123 K<sup>35</sup> but not for *N*-methyl-*N*-propylpyrrolidinium iodide<sup>36</sup> (it should be noted that different authors use other criteria to designate a specific interaction as a “hydrogen bond”). Anderson et al. observed weak hydrogen bonds in the crystal structure of a hydrated dicationic pyrrolidinium ionic liquid.<sup>37</sup> In our previous work considering thermotropic *N*-alkyl-*N*-methylpyrrolidinium liquid crystals, it was observed that the bromide salts with an alkyl chain of at least 11 carbon atoms exhibited T phases, and that the long-chain homologues showed an additional SmA phase.<sup>5</sup>

In this Article, we extend our study of liquid-crystalline pyrrolidinium compounds to salts that contain a mesogenic group, attached via a flexible alkyl spacer to the cationic core. Some of us showed that this approach can lead to nematic ionic liquid crystals (by attaching a sufficient number of rigid moieties with polar cyano substituents) as well as luminescent, high coordination number tetrakis  $\beta$ -diketonate lanthanidomesogens.<sup>12</sup> To obtain stable mesophases, the bulky lanthanide-containing anion should be counterbalanced by a cation with a large molecular area, and this cannot be achieved by cations with only long alkyl chains. Therefore, we extended our work to pyrrolidinium salts and metal complexes with mesogenic moieties. Furthermore, tilted smectic phases (such as SmC, SmF, and SmI phases) cannot be obtained with compounds that do not contain a rigid part.<sup>38</sup> Different anions, namely, bromide, bis(trifluoromethylsulfonyl)imide, tetrakis(2-thenoyltrifluoroaceto-nato)europeate(III), and tetrabromouranyl anions, were used. The influence of the type of mesogenic unit, the lengths of the flexible spacer and terminal alkyl chain, the size of the mesogenic group, and the type of anion on the mesomorphic behavior was investigated, as well as the detailed molecular packing within the different mesophases. The europium(III)-containing salts are of interest because of their excellent luminescence properties.<sup>5,12,39</sup> Mesomorphic, luminescent lanthanide complexes can be used to generate polarized luminescence.<sup>40</sup> The uranyl-containing salts have been shown to be not luminescent in the pure form (luminescence can, however, be induced by dissolution in a suitable organic solvent or in an ionic liquid); these salts are interesting from a fundamental point of view because of the incorporation of a metal-containing anion with an octahedral coordination geometry instead of the well-known tetrahedral or square-planar [MX<sub>4</sub>]<sup>2−</sup> anions (M<sup>2+</sup> = Cu<sup>2+</sup>, Pd<sup>2+</sup>, ...; X<sup>−</sup> = Cl<sup>−</sup>, Br<sup>−</sup>, I<sup>−</sup>).<sup>5</sup>

## Experimental Section

**General.** Defect textures of the mesophases were observed with an Olympus BX60 polarizing microscope equipped with a

LINKAM THMS600 hot stage and a LINKAM TMS93 programmable temperature controller. Microscope glass slides were immersed in a concentrated HNO<sub>3</sub> solution for 1 h, washed with distilled water, and finally rinsed with acetone which was then allowed to evaporate. Differential scanning calorimetry traces were recorded with a Mettler-Toledo DSC822e module (heating/cooling rate of 10 °C min<sup>−1</sup>; He atmosphere). The thermal stability was assessed by thermogravimetry in the range from 25 to 400 °C, at a heating rate of 10 °C min<sup>−1</sup>, under nitrogen, with a TA Instruments SDT Q600 thermal analyzer. Powder X-ray diffractograms were recorded with a Bruker AXS D8 Discover diffractometer mounted with a copper X-ray ceramic tube, working at 1.6 kW. The emitted Cu K $\alpha$  radiation ( $\lambda$  = 1.5418 Å) was focused on the sample by a Göbel mirror. All the samples (without a thermal history) were prepared by spreading the powders on a thin cleaned silicon wafer. Diffractograms were collected using the Bragg–Brentano reflection geometry ( $\theta/2\theta$  setup) at an angular resolution (in  $2\theta$ ) of 0.03° per step. The deviation between the temperature on the surface of the sample holder and the set temperature was about 3%. The scattered signal was recorded with a one-dimensional detector (LynxEye detector). Indexation of the powder X-ray diffractograms was performed with the WinXz<sup>POW</sup> program package, with the Index & Refine program using Werner's TREOR algorithm program (allowed 2θ error in matching the experimentally observed peaks = 0.05°).<sup>41,42</sup>

**Crystallography.** Small yellow single crystals of compound **6d** were obtained after 3 days by slowly evaporating a solution of the compound in water. Since no single crystals of a suitable size for in-house X-ray diffraction could be obtained, X-ray intensity data were collected at a synchrotron facility. A single-crystal with dimensions of 0.02 × 0.01 × 0.01 mm<sup>3</sup> was used to collect a 93.8% complete data set at the Swiss-Norwegian Beamline (SNBL) BM01 of the European Synchrotron Radiation Facility (ESRF) in Grenoble, France. Data were collected on a MAR345 imaging plate detector with  $\lambda$  = 0.7700 Å, increment = 2°, and crystal-to-detector distance = 100 mm. The crystal was immediately flash-cooled under a liquid nitrogen cryo-stream at 120 K. Two data sets were collected using the same crystal with the same crystal-to-detector distance but with different orientations and a φ range = 148° and 158°, respectively. A total of 6655 unique reflections were observed for the merged data to a resolution of 0.77 Å ( $R_{\text{int}} = 0.058$ ). The images were interpreted and integrated with the program CrysAlisPro from Oxford Diffraction.<sup>43</sup> The structure was solved by direct methods and refined by full-matrix least-squares on  $F^2$  using the SHELXTL program package.<sup>44</sup> Non-hydrogen atoms were anisotropically refined, and the hydrogen atoms in the riding mode with isotropic temperature factors were fixed at 1.2 times  $U(\text{eq})$  of the parent atoms (1.5 times for methyl groups). **6d:** C<sub>64</sub>H<sub>80</sub>Br<sub>4</sub>N<sub>2</sub>O<sub>10</sub>U,  $M = 1594.97 \text{ g mol}^{-1}$ , triclinic,  $P\bar{1}$  (no. 2),  $a = 10.1444(16)$  Å,  $b = 11.5777(6)$  Å,  $c = 15.703(3)$  Å,  $\alpha = 69.177(11)$ °,  $\beta = 86.343(13)$ °,  $\gamma = 65.638(11)$ °,  $V = 1562.9(4)$  Å<sup>3</sup>,  $T = 120(2)$  K,  $Z = 1$ ,  $\rho_{\text{calc.}} = 1.695 \text{ g cm}^{-3}$ ,  $\mu(\text{Cu K}\alpha) = 9.459 \text{ mm}^{-1}$ ,  $F(000) = 790$ , crystal size = 0.02 × 0.01 × 0.01 mm<sup>3</sup>, 6655 independent reflections ( $R_{\text{int}} = 0.058$ ). Number of parameters = 369. Final  $R = 0.0380$  for 6061 reflections with  $I > 2\sigma(I)$  and  $\omega R2 = 0.1220$  for all data. CCDC-723107 contains the supplementary crystallographic data for this paper. These data can be obtained free of charge from The Cambridge Crystallographic Data Centre (12 Union Road, Cambridge CB2 1EZ, U.K.; fax +44-1223-336033) via [www.ccdc.cam.ac.uk/data\\_request/cif](http://www.ccdc.cam.ac.uk/data_request/cif).

(34) Laus, G.; Bentivoglio, G.; Kahlenberg, V.; Griesser, U. J.; Schottenberger, H.; Nauer, G. *CrystEngComm* **2008**, *10*, 748–752.

(35) Golding, J.; Hamid, N.; MacFarlane, D. R.; Forsyth, M.; Forsyth, C.; Collins, C.; Huang, J. *Chem. Mater.* **2001**, *13*, 558–564.

(36) Babai, A.; Mudring, A. V. *Acta Crystallogr., Sect. E: Struct. Rep. Online* **2005**, *61*, o2913–o2915.

(37) Anderson, J. L.; Ding, R. F.; Ellern, A.; Armstrong, D. W. *J. Am. Chem. Soc.* **2005**, *127*, 593–604.

(38) Tschierske, C. *J. Mater. Chem.* **1998**, *8*, 1485–1508.

(39) Binnemans, K. Rare-Earth Beta-Diketonates. In *Handbook on the Physics and Chemistry of Rare Earths*; Gschneidner, K. A., Jr., Bünzli, J.-C. G., Pecharsky, V. K., Eds.; Elsevier: Amsterdam, 2005; pp 107–272.

(40) Galyametdinov, Y. G.; Knyazev, A. A.; Dzhabarov, V. I.; Cardinaels, T.; Driesen, K.; Görller-Walrand, C.; Binnemans, K. *Adv. Mater.* **2008**, *20*, 252–257.

(41) *WinX<sup>POW</sup>*, version 1.06; STOE & Cie GmbH: Darmstadt, Germany, 1999.

(42) Werner, P. E.; Eriksson, L.; Westdahl, M. *J. Appl. Crystallogr.* **1985**, *18*, 367–370.

(43) *Oxford Diffraction ABSPACK and CrysAlisPro*; Oxford Diffraction Ltd.: Oxford, United Kingdom, 2006.

(44) *SHELXTL-PC*, version 5.1; Bruker Analytical X-ray Systems Inc.: Madison, WI, 1997.

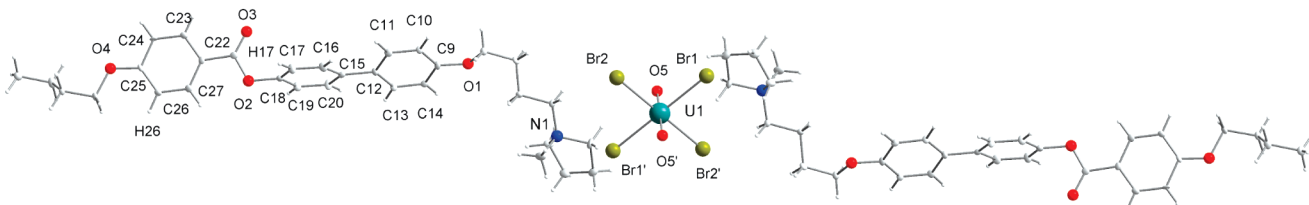


**Figure 1.** Detail of the crystal structure of compound **6d**, showing a  $[\text{UO}_2\text{Br}_4]^{2-}$  dianion surrounded by two *N*-[4-[4'-(4-butyloxybenzoyloxy)biphenyl-4-yloxy]butyl]-*N*-methylpyrrolidinium cations.

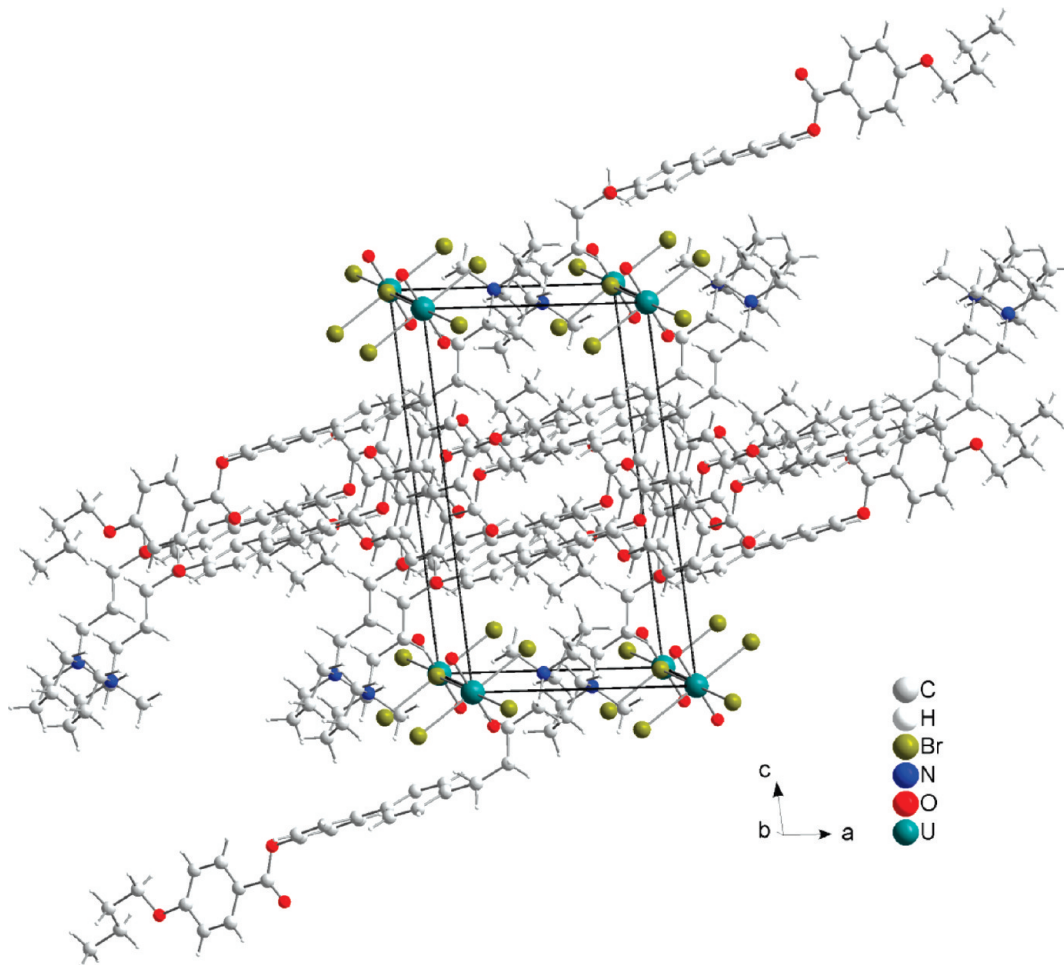


**Figure 2.** Packing in the crystal structure of compound **6d**, viewed along the *b* axis.

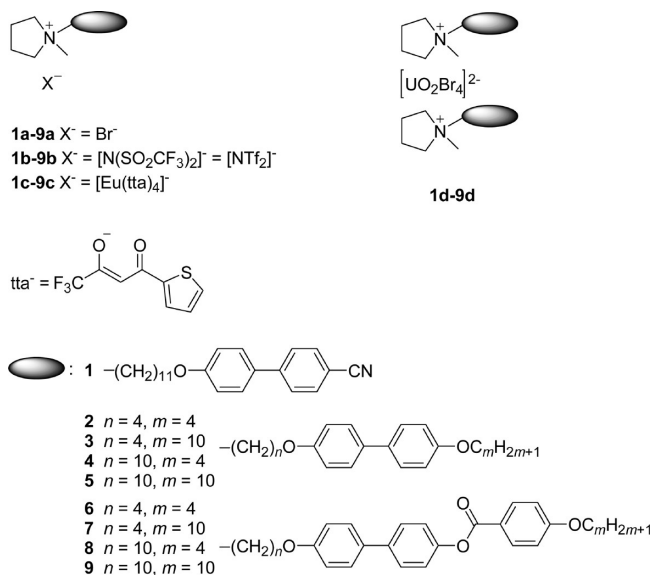
## Results and Discussion

**Single Crystal X-ray Diffraction.** Small crystals, suitable for single crystal X-ray structure determination, could be obtained for the uranyl complex **6d** by slowly evaporating a solution of the compound in water. The structure consists of *N*-[4-[4'-(4-butyloxybenzoyloxy)biphenyl-4-yloxy]butyl]-*N*-methylpyrrolidinium cations and  $[\text{UO}_2\text{Br}_4]^{2-}$  anions (Figure 1). The uranium atoms are located at the corners of the triclinic unit cell. In the first coordination sphere, the uranyl ion is surrounded by four bromide ions in the equatorial plane. In the packing of the crystal structure of compound **6d**, the cationic head groups and the  $[\text{UO}_2\text{Br}_4]^{2-}$  anions are arranged in layers parallel to (001) (Figure 2). The ionic sublayers are separated by the mesogenic parts of the cations, which are stacked in a parallel and interdigitated fashion. Intermolecular edge-to-face interactions between the aromatic rings are found (distance C(17)–H(17) to centroid (C(22)–C(27)) = 2.66 Å; distance C(26)–H(26) to

centroid (C(9)–C(14)) = 2.76 Å). It is remarkable that *monolayers* of  $[\text{UO}_2\text{Br}_4]^{2-}$  anions are formed, while *double layers* of  $[\text{UO}_2\text{Br}_4]^{2-}$  anions were observed in the single crystal structure of the *N*-methyl-*N*-tetradecylpyrrolidinium tetrabromouranyl salt.<sup>5</sup> As will be discussed in the section about powder X-ray diffraction, this monolayer structure continues to exist in the smectic A mesophase shown by compound **6d** at high temperatures.

**Thermal Behavior.** An overview of all the pyrrolidinium compounds that were investigated is shown in Scheme 1. The thermal properties of all the compounds were examined by polarizing optical microscopy (POM), differential scanning calorimetry (DSC), and X-ray diffraction on powder samples (PXRD). The transition temperatures and thermal data for all the pyrrolidinium salts are summarized in Table 1. Representative DSC traces can be found in the Supporting Information.

The pyrrolidinium bromide compounds are not stable at temperatures above approximately 225 °C. This was confirmed

**Scheme 1. Overview of All the Pyrrolidinium Compounds**

by POM, by the fact that the baseline of the DSC thermogram alters above approximately 225 °C, and by thermogravimetry (TG) (see the Supporting Information). Therefore, the pyrrolidinium salts were heated to only 180 °C during the first heating run in order to obtain a matching and reproducible cooling run and a reproducible second heating run. In the first heating run, all the bromide salts showed a broad, endothermic transition. This was not the case for the bis(trifluoromethylsulfonyl)imide salts nor for the europium- and uranyl-containing compounds (for mesomorphic pyrrolidinium bromides with long alkyl chains, this transition was not observed either<sup>5</sup>). This broad transition was not observed anymore in the second and third heating runs. The exact start and end temperatures of these transitions differed from one compound to another but were situated between 30 and 120 °C. Thermogravimetric measurements showed that these endothermic transitions most likely correspond to dehydration of the samples. From the thermograms presented in the Supporting Information, it is clear that the thermal stability of the salts is mainly determined by the type of anion. All the bromide salts start to decompose above 225–235 °C, irrespective of the exact structure of the incorporated mesogenic group. On the other hand, the bis(trifluoromethylsulfonyl)imide analogue of **3a**, compound **3b**, only decomposes above 340 °C. The metal-containing compounds **3c** and **3d** are also more stable than their bromide analogues (but less stable than compound **3b**).

The cyanobiphenyl-containing bromide salt, compound **1a**, showed only a monotropic SmA phase, just like the imidazolium analogue.<sup>12</sup> Surprisingly, the bromide salts with two aromatic rings and a short terminal alkyl chain ( $C_4$ ), compounds **2a** and **4a**, were not mesomorphic. On cooling from the isotropic liquid, compound **2a** showed a transition to a monotropic, optically uniaxial mesophase, immediately followed by a transition to an unstable monotropic, optically biaxial mesophase and subsequently by crystallization. Yoshizawa et al. reported that both 1-methyl-3-[8-(4'-butyloxybiphenyl-4-yloxy)octyl]imidazolium bromide and 1-methyl-3-[12-(4'-butyloxybiphenyl-4-yloxy)dodecyl]imidazolium bromide show a crystal smectic E phase over a broad temperature range, followed by a SmA phase.<sup>45</sup> Lattermann and co-workers showed that

*N*-[6-(4'-propyloxybiphenyl-4-yloxy)hexyl]pyridinium bromide and *N*-[10-(4'-propyloxybiphenyl-4-yloxy)decyl]pyridinium bromide exhibit a SmA phase, and both a crystal smectic E phase and SmA phase, respectively.<sup>16</sup> Our observations clearly illustrate the impact of the type of cationic head group on the mesomorphic behavior of ionic compounds. While it was expected that a microphase separation between the ionic head groups, the flexible alkyl spacers, the biphenyl moieties, and the terminal chains would lead to the formation of stable smectic mesophases, no mesomorphism was observed at all. On the other hand, the corresponding bromide salts with a long terminal alkyl chain ( $C_{10}$ ), compounds **3a** and **5a**, did show enantiotropic mesophases. Both compounds exhibited a crystal smectic E phase (see the sections about POM and PXRD) as well as a SmA phase. In the case of **5a**, a SmC phase was observed over a very narrow temperature range between the E phase and the SmA phase, but this transition was not detected by DSC and the phase could not be thoroughly investigated. The corresponding pyridinium salt, *N*-[10-(4'-decyloxybiphenyl-4-yloxy)decyl]pyridinium bromide, only shows a tilted SmC phase over a narrower temperature range.<sup>16</sup> Apparently, the replacement of a pyridinium ring (carrying a delocalized positive charge) by a pyrrolidinium ring (carrying a positive point charge) results in increased order, that is, a crystal smectic E phase instead of a disordered SmC phase. An elongation of the rigid core with one aromatic ring (toward a total of three aromatic rings) induces mesomorphism in the case of the bromide salts with a short terminal alkyl chain ( $C_4$ ): both compounds **6a** and **8a** showed a SmA phase, albeit at rather high temperatures. An extended rigid core in combination with a long terminal alkyl chain ( $C_{10}$ ) leads to an interesting phase behavior for compounds **7a** and **9a**. These salts showed an unidentified crystal smectic phase (designated as X) and a crystal smectic E phase, followed by a SmC phase and finally a SmA phase at high temperatures.

It is interesting to notice that no crystal smectic T phases were observed for bromide salts **1a**–**9a**, in contrast to the *N*-alkyl-*N*-methylpyrrolidinium bromide salts (which show T phases starting from an alkyl chain length of eleven carbon atoms; from a chain length of 18 carbon atoms, the T phase is followed by a high-temperature SmA phase).<sup>5</sup> For the *N*-alkyl-*N*-methylpyrrolidinium compounds, only localized Coulombic interactions have to be taken into account, as the cations do not carry any functional groups. For compounds **1a**–**9a**, interactions between the attached aromatic moieties are possible. However, as will be discussed in the section about powder X-ray diffraction, the molecular packing in the mesophases is still mainly determined by the strong electrical interactions. The influence of the mesogenic groups seems to be limited to excluded volume and space-filling effects. Nevertheless, the incorporation of a mesogenic unit leads to a larger variety of smectic mesophases than obtained for the *N*-alkyl-*N*-methylpyrrolidinium bromides, including SmA and SmC phases as well as ordered smectic phases (crystal smectic E and the unidentified X phases). Ordered smectic phases were only observed for the bromide salts with a long terminal alkyl chain.

As expected, bis(trifluoromethylsulfonyl)imide salts **1b**–**8b** exhibited lower melting points than the corresponding bromide salts. This is due to the decreased packing efficiency caused by the larger size of, and the charge delocalization in the bis(trifluoromethylsulfonyl)imide anion.<sup>5,11,12,46</sup> However, the bis

(45) Yoshizawa, H.; Mihara, T.; Koide, N. *Mol. Cryst. Liq. Cryst.* **2004**, *423*, 61–72.

(46) Yoshio, M.; Ichikawa, T.; Shimura, H.; Kagata, T.; Hamasaki, A.; Mukai, T.; Ohno, H.; Kato, T. *Bull. Chem. Soc. Jpn.* **2007**, *80*, 1836–1841.

**Table 1. Transition Temperatures and Thermal Data for the Pyrrolidinium Salts**

compound	anion	transition <sup>a</sup>	T/°C <sup>b</sup>	ΔH/kJ mol <sup>-1</sup> (ΔS/J K <sup>-1</sup> mol <sup>-1</sup> )
<b>1a</b>	Br <sup>-</sup>	(I → SmA) Cr → I	86 148	— <sup>c</sup> 32.8 (78)
<b>2a</b>	Br <sup>-</sup>	(M <sub>2</sub> → M <sub>1</sub> ) (I → M <sub>2</sub> ) Cr → I	142 143 166	— <sup>c</sup> — <sup>c</sup> 28.2 (64)
<b>3a</b>	Br <sup>-</sup>	Cr <sub>1</sub> → Cr <sub>2</sub> Cr <sub>2</sub> → E E → SmA <sup>d</sup>	98 143 159	4.4 (12) 5.7 (14) 15.9 (37)
<b>4a</b>	Br <sup>-</sup>	Cr → I	179	29.1 (64)
<b>5a</b>	Br <sup>-</sup>	Cr <sub>1</sub> → Cr <sub>2</sub> Cr <sub>2</sub> → E E → SmA <sup>f</sup> SmA → I	72 <sup>e</sup> 125 162 197	3.2 (9) 1.6 (4) 16.9 (39) 1.4 (3)
<b>6a</b>	Br <sup>-</sup>	Cr <sub>1</sub> → Cr <sub>2</sub> Cr <sub>2</sub> → Cr <sub>3</sub> Cr <sub>3</sub> → SmA <sup>d</sup>	59 <sup>e</sup> 103 <sup>e</sup> 208	3.6 (11) 0.5 (1.4) 26.5 (55)
<b>7a</b>	Br <sup>-</sup>	Cr <sub>1</sub> → Cr <sub>2</sub> Cr <sub>2</sub> → Cr <sub>3</sub> Cr <sub>3</sub> → X X → E E → SmC SmC → SmA <sup>d</sup>	41 <sup>e</sup> 132 <sup>e</sup> 143 197 203 214	1.9 (6) 0.9 (2) 0.8 (2) 5.1 (11) 15.8 (33) 0.9 (1.8)
<b>8a</b>	Br <sup>-</sup>	Cr <sub>1</sub> → Cr <sub>2</sub> Cr <sub>2</sub> → Cr <sub>3</sub> Cr <sub>3</sub> → SmA SmA → I	108 <sup>e</sup> 122 196 215	1.2 (3) 1.6 (4) 21.7 (46) 3.6 (7)
<b>9a</b>	Br <sup>-</sup>	Cr → X X → E E → SmC SmC → SmA <sup>d</sup>	109 183 190 225	6.0 (16) 1.6 (3) 10.1 (22) 6.6 (13) <sup>g</sup>
<b>1b</b>	[NTf <sub>2</sub> ] <sup>-</sup>	<i>first heating/cooling cycle:</i> (I → SmA) Cr → I	15 56	— <sup>c</sup> 25.5 (77)
<b>2b</b>	[NTf <sub>2</sub> ] <sup>-</sup>	Cr → I	76	20.2 (58)
<b>3b</b>	[NTf <sub>2</sub> ] <sup>-</sup>	(I → SmA) Cr → I	60 80	— <sup>c</sup> 26.6 (75)
<b>4b</b>	[NTf <sub>2</sub> ] <sup>-</sup>	Cr <sub>1</sub> → Cr <sub>2</sub> Cr <sub>2</sub> → I	13 <sup>e</sup> 129	0.6 (2) 36.6 (91)
<b>5b</b>	[NTf <sub>2</sub> ] <sup>-</sup>	Cr → I	110	30.2 (79)
<b>6b</b>	[NTf <sub>2</sub> ] <sup>-</sup>	Cr <sub>1</sub> → Cr <sub>2</sub> Cr <sub>2</sub> → SmA SmA → I	33 <sup>e</sup> 101 114	7.9 (26) 15.8 (42) 4.3 (11)
<b>7b</b>	[NTf <sub>2</sub> ] <sup>-</sup>	Cr <sub>1</sub> → Cr <sub>2</sub> Cr <sub>2</sub> → SmA SmA → I	100 106 143	15.9 (43) 21.1 (56) 2.1 (5)
<b>8b</b>	[NTf <sub>2</sub> ] <sup>-</sup>	(I → SmA) Cr → I	148 154	5.9 (14) <sup>h</sup> 41.0 (96)
<b>9b</b>	[NTf <sub>2</sub> ] <sup>-</sup>	(SmC → M) <sup>i</sup> Cr → SmC SmC → SmA SmA → I	109 116 125 154	5.2 (14) <sup>j</sup> 19.6 (50) — <sup>c</sup> 10.4 (24) <sup>k</sup>
<b>1c</b>	[Eu(tta) <sub>4</sub> ] <sup>-</sup>	<i>first heating run:</i> g → I	47 <sup>e</sup>	6.1 (19)

Table 1. Continued

compound	anion	transition <sup>a</sup>	T/°C <sup>b</sup>	ΔH/kJ mol <sup>-1</sup> (ΔS/J K <sup>-1</sup> mol <sup>-1</sup> )
<b>3c</b>	[Eu(tta) <sub>4</sub> ] <sup>-</sup>	<i>first heating run:</i> Cr → I <i>second heating run:</i> g → I	136 34 <sup>c</sup>	77.1 (189) 6.6 (22)
<b>5c</b>	[Eu(tta) <sub>4</sub> ] <sup>-</sup>	<i>first heating run:</i> g → I	29 <sup>e</sup>	4.2 (14)
<b>6c</b>	[Eu(tta) <sub>4</sub> ] <sup>-</sup>	<i>first heating run:</i> Cr → I <i>second heating run:</i> g → I	59 55 <sup>e</sup>	7.8 (24) 2.8 (8)
<b>7c</b>	[Eu(tta) <sub>4</sub> ] <sup>-</sup>	<i>first heating run:</i> Cr → I <i>second heating run:</i> g → I	117 43 <sup>e</sup>	58.9 (151) 4.1 (13)
<b>1d</b>	[UO <sub>2</sub> Br <sub>4</sub> ] <sup>2-</sup>	Cr → I	172	76.6 (172)
<b>2d</b>	[UO <sub>2</sub> Br <sub>4</sub> ] <sup>2-</sup>	Cr → I <sup>f</sup>	103	33.3 (89)
<b>3d</b>	[UO <sub>2</sub> Br <sub>4</sub> ] <sup>2-</sup>	Cr → SmA <sup>d,m</sup>	112	63.5 (165)
<b>5d</b>	[UO <sub>2</sub> Br <sub>4</sub> ] <sup>2-</sup>	Cr <sub>1</sub> → Cr <sub>2</sub> Cr <sub>2</sub> → SmC SmC → SmA <sup>d</sup>	75 120 126	3.4 (10) 36.5 <sup>n</sup>
<b>6d</b>	[UO <sub>2</sub> Br <sub>4</sub> ] <sup>2-</sup>	Cr → SmA <sup>d</sup>	219	110.9 (225)
<b>7d</b>	[UO <sub>2</sub> Br <sub>4</sub> ] <sup>2-</sup>	(SmA → SmC) Cr → SmA <sup>d</sup>	183 185	— <sup>c</sup> 43.8 (95)
<b>8d</b>	[UO <sub>2</sub> Br <sub>4</sub> ] <sup>2-</sup>	Cr <sub>1</sub> → Cr <sub>2</sub> Cr <sub>2</sub> → SmA SmA → I	86 <sup>e</sup> 205 237	18.0 (50) 67.0 (140) 7.0 (14)
<b>9d</b>	[UO <sub>2</sub> Br <sub>4</sub> ] <sup>2-</sup>	Cr <sub>1</sub> → Cr <sub>2</sub> Cr <sub>2</sub> → SmF/SmI <sup>o</sup> SmF/SmI → SmC SmC → SmA <sup>d</sup>	118 158 201 223	1.8 (5) 18.6 (43) 9.2 (20) 8.0 (16)

<sup>a</sup> Abbreviations: g = glass; Cr, Cr<sub>1</sub>, Cr<sub>2</sub>, and Cr<sub>3</sub> = crystalline phase; M, M<sub>1</sub>, and M<sub>2</sub> = unidentified smectic phase; X = unidentified highly ordered smectic phase (= crystal smectic G, J, H, or K phase); E = crystal smectic E phase; SmI = smectic I phase, SmF = smectic F phase; SmC = smectic C phase; SmA = smectic A phase; I = isotropic liquid. Transitions between brackets indicate transitions to a monotropic mesophase. <sup>b</sup> Onset temperatures obtained by DSC at heating/cooling rates of 10 °C min<sup>-1</sup> (He atmosphere). Values were taken from the second heating run, unless indicated otherwise. The compounds were mostly heated to 180 °C during the first heating run and cooled down to -20 °C during the first cooling run. <sup>c</sup> Not detected by DSC. The transition temperature was determined by POM (for a monotropic mesophase, the temperature at which the monotropic phase transformed into the isotropic liquid phase or the following mesophase on heating is reported). <sup>d</sup> The exact clearing point could not be reliably determined due to partial decomposition above 225–235 °C. <sup>e</sup> Peak temperature. <sup>f</sup> Between the crystal smectic E phase and the SmA phase, a SmC phase was observed over a very narrow temperature range. <sup>g</sup> This enthalpy change associated with the SmC → SmA transition is relatively large in comparison to literature values. However, even higher values were observed before for ionic liquid crystals.<sup>16</sup> The enthalpy change appears to be highly dependent on both the cation type and the anion type, as compounds **7a** and **9b** showed a small enthalpy change at the transition from the SmC phase to the SmA phase.

<sup>h</sup> By DSC, this transition was only observed in the cooling runs. At 140 °C, a second exothermic peak was observed in the cooling runs, corresponding to crystallization of the monotropic mesophase ( $\Delta H = -32.0 \text{ kJ mol}^{-1}$ ;  $\Delta S = -77 \text{ J K}^{-1} \text{ mol}^{-1}$ ). <sup>i</sup> The unidentified monotropic M phase is probably a SmF phase (see the section about POM). <sup>j</sup> By DSC, this transition was only observed in the cooling runs. On further cooling, a broad glass transition was observed at an onset temperature of 93 °C ( $\Delta H = -3.2 \text{ kJ mol}^{-1}$ ;  $\Delta S = -9 \text{ J K}^{-1} \text{ mol}^{-1}$ ). <sup>k</sup> This enthalpy change associated with isotropization is relatively large in comparison to literature values for SmA → I enthalpy changes (4–6 kJ mol<sup>-1</sup>). This may be caused by the breakdown of the order in systems having strong interactions, such as the strong ionic interactions in the investigated pyrrolidinium salts.<sup>16</sup> <sup>l</sup> Before this endothermic transition, an exothermic recrystallization process took place at 76 °C (peak temperature) ( $\Delta H = -37.3 \text{ kJ mol}^{-1}$ ;  $\Delta S = -107 \text{ J K}^{-1} \text{ mol}^{-1}$ ). <sup>m</sup> Before this endothermic transition, an exothermic recrystallization process took place at 80 °C (peak temperature) ( $\Delta H = -4.2 \text{ kJ mol}^{-1}$ ;  $\Delta S = -12 \text{ J K}^{-1} \text{ mol}^{-1}$ ). <sup>n</sup> As the transition peaks in the DSC thermogram were not fully resolved, the total enthalpy value, ΔH, for both transitions is given. <sup>o</sup> No unequivocal phase type assignment was possible (see the sections about POM and about PXRD).

(trifluoromethylsulfonyl)imide salt with a long alkyl spacer (C<sub>10</sub>) and a long terminal alkyl chain (C<sub>10</sub>), compound **9b**, showed a slightly higher melting point than the corresponding bromide salt **9a**. This illustrates the fact that, as the size of the nonionic part of the compound increases, the influence of the anion size on the melting point decreases when comparing the transition temperatures of series **2a–9a** and **2b–9b**. Although in general a lower melting point could be achieved by incorporation of

a bis(trifluoromethylsulfonyl)imide anion, the mesomorphic properties did not improve. Due to the larger size of the [NTf<sub>2</sub>]<sup>-</sup> anion, a larger mesogenic group is required to obtain a balance in molecular area between the ionic head groups and the mesogenic moieties, which is necessary to form a stable smectic mesophase. The cyanobiphenyl-containing [NTf<sub>2</sub>]<sup>-</sup> salt, compound **1b**, only showed a monotropic SmA phase. The salt was obtained as a colorless, supercooled liquid. On cooling

below room temperature, the metastable SmA phase appeared. After several months, the supercooled liquid crystallized. A similar phase behavior was observed for the corresponding imidazolium salt.<sup>12</sup> Compounds **2b**, **4b**, and **5b** were not mesomorphic, while compound **3b** only showed a monotropic SmA phase. On the other hand, the bis(trifluoromethylsulfonyl)imide salts with a longer rigid aromatic core, compounds **6b–9b**, were all mesomorphic, but the mesophase temperature ranges were small in comparison to those of the corresponding bromide salts. Although salt **6b** contains a short terminal alkyl chain ( $C_4$ ), the short spacer allows the existence of an enantiotropic SmA phase, albeit over a rather narrow temperature range. For compound **8b**, only a monotropic SmA phase was observed. Compound **7b** showed an orthogonal SmA phase but no tilted smectic phase, in contrast to bromide salt **7a**. On the other hand, compound **9b**, containing a long alkyl spacer, exhibited a SmC phase between 116 and 125 °C. On cooling below the melting point, the transition from the SmC phase to a monotropic mesophase was observed. Although this phase could not be unequivocally identified, it is probably a tilted SmF or SmI phase (these phases occur most frequently below a higher-temperature SmC phase, as they are the hexagonally ordered analogues of the latter phase<sup>47,48</sup>). This phase type assignment is supported by the observed enthalpy change and viscosity and also by the defect texture observed by POM (see below). It should be mentioned that *N*-octadecyl-*N*-methylpyrrolidinium bis(trifluoromethylsulfonyl)imide<sup>5</sup> and 1-methyl-3-octadecylimidazolium bis(trifluoromethylsulfonyl)imide<sup>11</sup> are not liquid-crystalline.

It is clear that the introduction of the bulky, asymmetric bis(trifluoromethylsulfonyl)imide anion inhibits the formation of crystal smectic phases: compounds **1b**, **3b**, and **6b–9b** only showed low-ordered SmC and SmA phases (except for the tilted monotropic mesophase M additionally shown by **9b**). In this aspect, it was also found that *N*-octadecyl-*N*-methylpyrrolidinium bromide showed a highly ordered crystal smectic T phase and a high-temperature SmA phase while the corresponding thiocyanate salt only showed a SmA phase.<sup>5</sup>

Unfortunately, the luminescent tetrakis(2-thenoyl trifluoroacetato)euporate(III) complexes **1c–7c** were not liquid-crystalline. The compounds were obtained as pale yellow powders, and on cooling from the isotropic liquid phase a low-melting glass was formed. Compounds **1c** and **5c** were immediately obtained as a glass. It was expected that the compounds containing a cation with an extended rigid core, separated from the ionic head group by a long alkyl spacer, would be mesomorphic: the bulky metal-containing anion should be counterbalanced by the relatively large, decoupled mesogenic moiety. We did not succeed to obtain complexes **8c** and **9c** in a sufficiently high purity (see the Supporting Information). Since the pure europium(III) compound **7c** was not liquid-crystalline, we tried to exploit the mesomorphic properties of the corresponding pyrrolidinium bromide, compound **7a**, as well as the luminescence properties of **7c** by mixing these two compounds in different molar ratios (the two components were dissolved in  $CH_2Cl_2$ , the mixture was sonicated for 2 min, and then the solvent was removed under reduced pressure, after which the mixture was dried *in vacuo* at 50 °C). For mole percentages of **7c** lower than about 15% (corresponding to a mass percentage of about 30%), a

homogeneous mixture was obtained: no phase separation was detected by POM or DSC. A doping concentration of about 30 wt % is quite high; it is our experience that the solubility of lanthanide  $\beta$ -diketonate complexes in common liquid-crystalline materials such as 5CB or MBBA is only a few wt %.<sup>49</sup> While a mixture of **7a** and **7c** in a 99:1 molar ratio showed a Cr-X-E-SmC-SmA phase sequence, no SmC phase was exhibited by mixtures of **7a** and **7c** in 95:5, 90:10, ... molar ratios. All the homogeneous mixtures showed an intense red photoluminescence with high color purity. The luminescence spectra at room temperature (see below) were similar to the spectra already reported for analogous tetrakis(2-thenoyl trifluoroacetato)euporate(III) complexes.<sup>12</sup>

In the tetrabromouranyl salts **1d–9d**, two pyrrolidinium cations are combined with a  $[UO_2Br_4]^{2-}$  dianion. We recently reported on this type of complexes with a pseudo-octahedral metal-containing anion.<sup>5</sup> While analogous compounds with tetrahedral or square-planar  $[MX_4]^{2-}$  anions ( $M^{2+} = Cu^{2+}$ ,  $Pd^{2+}$ ,  $Co^{2+}$ ,  $Ni^{2+}$ ,  $Zn^{2+}$ ,  $Cd^{2+}$ , ...;  $X^- = Cl^-$ ,  $Br^-$ ,  $I^-$ ) and cations with only long alkyl chains are well-known,<sup>10,17,50–53</sup> these tetrahalometallate anions have never, to the best of our knowledge, been combined with cations bearing a mesogenic group. All complexes showed enantiotropic SmA phases, except for the cyanobiphenyl-containing complex, compound **1d**, and for the compound with a two-ring mesogenic group and a short spacer and short terminal alkyl chain, compound **2d**. Unfortunately, complex **4d** could not be obtained in a pure form. Like in the case of the bromide salts, the complexes with an extended rigid core in combination with a long terminal alkyl chain ( $C_{10}$ ), compounds **7d** and **9d**, additionally showed a tilted SmC phase (which was only monotropic in the case of **7d**). Complex **9d** also showed a SmF or SmI phase. Interestingly, complex **5d** showed a SmC phase over a rather narrow temperature range, while this was not the case for the corresponding bromide salt.

The phase behavior of compounds **1d–9d** can be compared with the mesomorphic behavior of the *N*-alkyl-*N*-methylpyrrolidinium tetrabromouranyl salts. The latter compounds show highly ordered crystal smectic E phases when the alkyl chain contains 14 or more carbon atoms (and additionally a higher-temperature SmA phase in the case of the very long alkyl chains).<sup>5</sup> In contrast, the mesomorphic tetrabromouranyl salts that are presented here all show low-ordered SmA and SmC phases (and also a SmF/SmI phase in the case of **9d**). Apparently, the mesogenic moieties are not compatible with ordered mesophase structures when combined with the  $[UO_2Br_4]^{2-}$  dianion, while some of the corresponding bromide salts do show ordered smectic phases (see above).

The SmA phases could be easily identified by POM on the basis of their defect textures: focal conic fan and oily streak textures (Figure 3a and 3c, respectively; see also the Supporting Information, Figures S9 and S10) were observed. Large homeotropic domains were seen as well. The SmA phases of compounds **3a** and **5a** appeared spontaneously in their focal conic texture, while the SmA phases of compounds **7a** and **9a** were mostly observed in their oily streak texture. In some cases, it was possible to obtain

(49) Binnemans, K.; Moors, D. *J. Mater. Chem.* **2002**, *12*, 3374–3376.

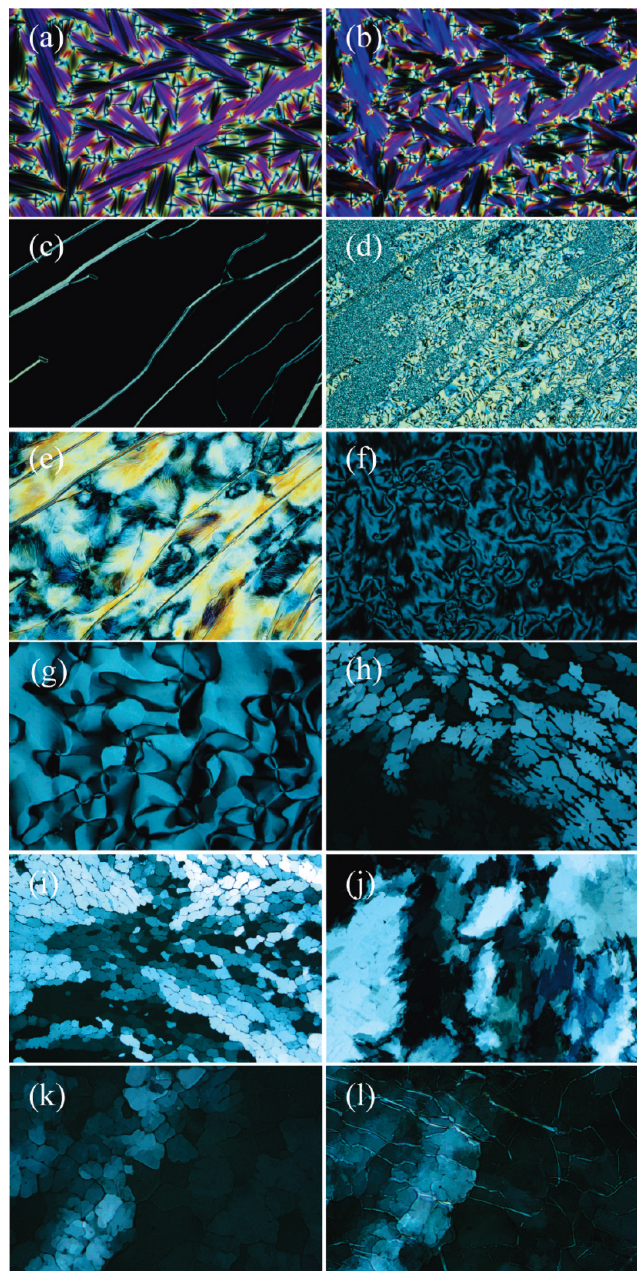
(50) Neve, F.; Crispini, A.; Armentano, S.; Francescangeli, O. *Chem. Mater.* **1998**, *10*, 1904–1913.

(51) Hardacre, C.; Holbrey, J. D.; McCormac, P. B.; McMath, S. E. J.; Nieuwenhuyzen, M.; Seddon, K. R. *J. Mater. Chem.* **2001**, *11*, 346–350.

(52) Neve, F.; Francescangeli, O.; Crispini, A. *Inorg. Chim. Acta* **2002**, *338*, 51–58.

(53) Lee, C. K.; Peng, H. H.; Lin, I. J. B. *Chem. Mater.* **2004**, *16*, 530–536.

homeotropically aligned samples using chemically cleaned glass slides. The transition from the SmA phase to the SmC phase was accompanied by the disappearance of the homeotropic domains and the appearance of a typical Schlieren texture with four-brushes point defects (Figure 3d and 3f). On cooling from a SmA phase exhibiting a focal conic fan texture, the fan shapes transformed into *broken* fans, while the focal conics became less pronounced (Figure 3b, compare with Figure 3a). The SmF/SmI phase shown by uranyl complex **9d** was characterized by the appearance of a Schlieren-mosaic texture on cooling from the SmC phase and by a rather low viscosity (certainly much lower than the viscosity of, e.g., the E phase shown by compound **3a**). This excluded the possibility of a crystal smectic phase, which was confirmed by powder X-ray diffraction measurements (see below). Pseudohomeotropic domains could be observed: by simultaneously rotating both polarizers of the microscope, the apparently homeotropic areas showed a defect texture, indicating a tilted mesophase. Because a Schlieren-mosaic texture was observed, rather than true Schlieren brushes



arising from point singularities, the phase is probably a SmF phase.<sup>47</sup> Figure 3e shows a paramorphotic texture of the phase, obtained on cooling from the higher-temperature SmA and SmC phases (Figure 3c and 3d, respectively) (remains of the oily streaks from the SmA phase are clearly visible). Figure 3g displays the Schlieren-mosaic texture exhibited by the monotropic mesophase shown by compound **9b** on cooling from the SmC phase. This monotropic mesophase is probably also a SmF phase. The crystal smectic E phases exhibited by compounds **3a** and **5a** were characterized by the dendritic growth of a mosaic platelet texture on cooling from the higher-temperature mesophase (Figure 3h and 3i). Some of the transparent platelets overlapped, giving ghostlike images of platelets; this texture is very characteristic of an E phase.<sup>47</sup> The bulk of the sample often displayed a noncharacteristic paramorphotic texture (see the Supporting Information, Figure S11). Small pseudo-homeotropic domains could sometimes be seen (it should be remembered that the E phase is an optically biaxial phase<sup>47</sup>). The phases were clearly soft and flowing, albeit more viscous than the SmA phases. The E phase type assignment was supported by powder X-ray diffraction measurements (see below). The phases shown by compounds **7a** and **9a** just below their SmC phase were also designated as crystal smectic E phases on the basis of the observed texture: on cooling, a platelet texture grew dendritically from the SmC phase, like in the case of compounds **3a** and **5a**. The Schlieren texture of the SmC phase completely disappeared, and ghostlike images of platelets could be seen again (shown in Figure 3k for **7a**), as well as pseudo-homeotropic areas. On further cooling, both E phases transformed into a viscous (but clearly flowing), highly ordered crystal smectic phase, designated as X. By POM, this transition could be seen as the appearance of ill-defined lines or bars in the platelet texture (Figure 3l). No conclusions about the phase type could be drawn from this observation. However, considering the well-known thermodynamic order of the different mesophase types and assuming that no hitherto unknown smectic phases are involved, these mesophases are expected to be crystal smectic H or K phases (indeed, on cooling a hypothetical calamitic liquid crystal showing all types of smectic

**Figure 3.** Mesophase defect textures observed by POM: (a) focal conic fan texture of the SmA phase of **9b** at 126 °C (500× magnification); (b) broken focal conic fan texture of the SmC phase of **9b** at 119 °C (500× magnification); (c) oily streak texture of the SmA phase of **9d** at 224 °C (200× magnification); (d) Schlieren texture of the SmC phase of **9d** at 203 °C (200× magnification); (e) paramorphotic texture of the SmF/SmI phase of **9d** at 175 °C (200× magnification); (f) Schlieren texture of the SmC phase of **9b** at 117 °C (500× magnification); (g) Schlieren-mosaic texture of the monotropic M phase (probably a SmF phase) of **9b** at 105 °C, obtained on cooling from the SmC phase showing its typical Schlieren texture (500× magnification); (h) dendritic growth of the crystal smectic E phase of **3a** from the homeotropically aligned SmA phase at 152 °C (200× magnification); (i) mosaic platelet texture of the crystal smectic E phase of **3a** at 146 °C (100× magnification); (j) supercooled crystal smectic E phase of **3a** at 136 °C (200× magnification); (k) platelet texture of the crystal smectic E phase of **7a** at 200 °C (500× magnification); (l) paramorphotic texture of the crystal smectic X phase of **7a** at 175 °C (500× magnification). An identical sample area is shown in (a) and (b); (c), (d), and (e); (h) and (i); and (k) and (l) (the different phases were obtained consecutively on cooling from the isotropic liquid phase). For photographs (a) and (b), a cell with planar alignment layers was filled with compound **9b** by means of capillary action. Although homeotropic areas were excluded in this way, the molecules could not be oriented in one single direction.

mesophases, the following hypothetical phase sequence would occur: I → SmA → SmC → SmB → SmI → SmF → B → J → G → E → K → H → Cr.<sup>54</sup> The three-dimensionally correlated nature of the crystal smectic X phases was reflected by the presence of a number of (*hkl*) reflections in the wide-angle region of the powder X-ray diffractograms (see below). The formation of these phases on cooling was a kinetically slower process, due to the rather high viscosity.

**Comparison of Transition Temperatures.** Considering the series **2a–9a**, a lower melting point was achieved for the compounds with a long terminal alkyl chain ( $C_{10}$ ) in comparison to their analogues with a short terminal alkyl chain ( $C_4$ ) (see the Supporting Information, Figure S2). Except for compounds **2a** and **4a**, the compounds with a long alkyl spacer ( $C_{10}$ ) also showed lower melting points than their analogues with a short alkyl spacer ( $C_4$ ). The net result is that compound **9a**, containing both a long terminal alkyl chain and a long flexible alkyl spacer, showed the lowest melting point in the series **2a–9a**. It was not possible to determine the influence of the chain lengths on the mesophase temperature ranges, as decomposition often occurred before reaching the clearing point. The length of the terminal alkyl chain influenced not only the melting point but also the types of mesophases that were formed (to a greater extent than the spacer length did). With short terminal alkyl chains, only SmA phases were formed (or no enantiotropic mesophases were observed at all).

Considering the series **2b–9b**, it is not possible to pursue the conclusions drawn above. In this series, compound **6b**, containing a short terminal alkyl chain and a short alkyl spacer, showed the lowest melting point of the mesomorphic compounds (see the Supporting Information, Figure S3). For the compounds with short alkyl spacers (compounds **2b** and **3b**, and **6b** and **7b**), a longer terminal alkyl chain leads to a small *increase* of the melting point. This behavior is the opposite of the evolution observed for the bromide salts. On the other hand, for the compounds with long alkyl spacers (compounds **4b** and **5b**, and **8b** and **9b**), the influence of the terminal alkyl chain length is similar to that observed for the bromide salts.

While the tetrabromouranyl salts with two-ring mesogenic groups showed lower melting points than their bromide counterparts, the opposite behavior was observed for the salts with three-ring mesogenic groups in the series **2d–9d** (see the Supporting Information, Figure S4). In addition, a shorter mesogenic group clearly leads to much lower melting points. When comparing Supporting Information Figures S2 and S4, it is clear that the mesophase temperature ranges (considered between the melting point and 240 °C) are somewhat higher for the tetrabromouranyl salts than for the corresponding bromide salts (compare, e.g., **5a** and **5d**). This observation could be related to the presence of the *doubly* negatively charged  $[UO_2Br_4]^{2-}$  anions: it was already noted by Lin and co-workers that the clearing process involves mainly the collapse of the ionic sublayers. Therefore, stronger electrostatic interactions are expected to result in an increased clearing point.<sup>53</sup> It is interesting to note, however, that the *N*-alkyl-*N*-methylpyrrolidinium tetrabromouranyl salts only show larger mesophase ranges as compared to the corresponding bromide salts in the case of very long alkyl chains (more than 19 carbon atoms) (a similar behavior was observed for the 1-methyl-3-alkylimidazolium salts with  $[CoCl_4]^{2-}$  or  $[NiCl_4]^{2-}$  as anionic fragments).<sup>5,10</sup>

**Powder X-ray Diffraction.** The liquid-crystalline pyrrolidinium compounds were studied by X-ray diffraction on powder

samples for further identification of the enantiotropic mesophases and to obtain more information about the molecular packing within the mesophases. Table 2 gives an overview of the Bragg reflections collected from the X-ray diffractograms of compounds **3a**, **5a**, **6a**, **7a**, **9a**, **6b**, **7b**, **9b**, **3d**, **5d**, **6d**, **7d**, **8d**, and **9d** (no suitable X-ray diffraction data could be obtained for compound **8a**). The crystalline nature of the solid phases at room temperature was confirmed by the presence of several sharp Bragg reflections at both small and wide angles. In addition, the equidistant small-angle reflections indicated that the molecules are arranged into a lamellar structure. The diffractograms of the smectic mesophases show multiple sharp and equidistant reflections at small and medium angles in the case of the SmF/SmI phases and the ordered crystal smectic phases (E and X), or only up to three sharp and equidistant reflections at small angles in the case of the SmA and SmC phases. These reflections, indexed as (00*l*), are related to the consecution of the smectic layers of a specific layer thickness *d* (Table 2). The presence of multiple small-angle peaks (up to the ninth-order reflection, (009)) for many of the mesophases indicates that the positions of the strongly diffracting bromide anions *within* the smectic layers are quite well-defined in these phases. For all mesophases, a diffuse scattering halo centered at about 4.7–4.8 Å was observed in the wide-angle region (most clearly for the SmC and SmA phases). This broad signal corresponds to the lateral short-range order of the disordered (molten) aliphatic chains. Except for the SmA and SmC phases, multiple signals were additionally seen in the wide-angle region (see below). For instance, for the crystal smectic E phase shown by compound **3a**, two (rather weak) wide-angle reflections were observed. These indicate a two-dimensional ordering of the molecules within the smectic layers, and could be indexed as the (110) and (200) reflections of a two-dimensional centered rectangular lattice. The diffractograms of the crystal smectic X phases exhibited by compounds **7a** and **9a** showed a number of (*hkl*) reflections in the wide-angle region, indicative of an interlayer coupling and a long-range order within the layers. For a full characterization of these mesophases, X-ray diffraction experiments on aligned samples using a two-dimensional detector are required. This also applies to the distinction between a SmF and a SmI phase for compound **9d**. Unfortunately, no aligned samples could be obtained (see also the caption of Figure 3). In the case of the bis(trifluoromethylsulfonyl)imide salts **6b** and **7b**, a diffuse halo centered at about 6.8–7.2 Å was observed in the diffractogram. This signal corresponds to the short-range positional correlation of the  $[NTf_2]^-$  anions within the SmA layers (or, more precisely, within the ionic sublayers). For the uranyl complexes, a diffuse halo centered at about 7.7–8.2 Å could be observed, which corresponds to some lateral periodicity of the  $[UO_2Br_4]^{2-}$  dianions within the ionic sublayers (see below).<sup>5</sup>

As expected, the layer thickness, *d*, was found to decrease with increasing temperature for all the SmA phases (except for the SmA phase shown by **9b**, for which *d* remained more or less constant over the whole SmA temperature range), due to an increasing thermal mobility of the alkyl chains (see Supporting Information, Figure S12). In contrast, the layer thickness of the SmC phases increased with temperature, due to a decrease in the tilt angle toward the formation of the higher-temperature de Vries type SmA phases (see Supporting Information, Figure S13). The layer spacing of the viscous, highly ordered smectic phases was found to be rather independent of the temperature (see Supporting Information, Figure S13); indeed, for highly structured tilted smectic phases, such as the G, J, H, and K phases, the change in tilt angle as a function of the temperature is usually low.<sup>47</sup> As far as the SmA phases are concerned, the ratio *d/L* (with *L* being the

(54) Dierking, I. *Textures of Liquid Crystals*; Wiley-VCH: Weinheim, 2003.

**Table 2. Most Relevant Bragg Reflections Collected from the X-ray Diffractograms of the Different Enantiotropic Mesophases (an Extensive Table with All Observed Reflections, Including All (00*l*) Reflections with *l* > 3, Can Be Found in the Supporting Information)**

				<i>d</i> <sub>meas.</sub> / Å <sup>a</sup>	<i>I</i> <sup>b</sup>	<i>hkl</i> <sup>c</sup>	<i>d</i> <sub>calc.</sub> / Å <sup>a</sup>	parameters of smectic phase <sup>d–g</sup>
<b>3a</b>	42.29 VS 21.07 M — <sup>h</sup> 4.73 <sup>i</sup> VW 3.74 VW	001 002 003 110 200	42.15 21.08 <i>A</i> <sub>M</sub> = 47.2 Å <sup>2</sup> <i>a</i> = 7.48 Å <i>b</i> = 6.09 Å <i>c</i> = 42.15 Å <i>L</i> = 31.75 Å <i>d/L</i> = 1.33					E: <i>T</i> = 150 °C <i>V</i> <sub>M</sub> = 993 Å <sup>3</sup> <i>A</i> <sub>M</sub> = 47.2 Å <sup>2</sup> <i>a</i> = 7.48 Å <i>b</i> = 6.09 Å <i>c</i> = 42.15 Å <i>L</i> = 31.75 Å <i>d/L</i> = 1.33
	49.63 VS 24.81 W	001 002	49.63 24.81					SmA: <i>T</i> = 180 °C <i>V</i> <sub>M</sub> = 1013 Å <sup>3</sup> <i>A</i> <sub>M</sub> = 40.8 Å <sup>2</sup> <i>L</i> = 31.75 Å <i>d/L</i> = 1.56
<b>5a</b>	52.68 VS 26.11 M 17.46 S 4.62 W 4.12 VW	001 002 003 110 200	52.32 26.16 <i>A</i> <sub>M</sub> = 43.6 Å <sup>2</sup> <i>a</i> = 8.24 Å <i>b</i> = 5.58 Å <i>c</i> = 52.32 Å <i>L</i> = 38.77 Å <i>d/L</i> = 1.35					E: <i>T</i> = 145 °C <i>V</i> <sub>M</sub> = 1142 Å <sup>3</sup> <i>A</i> <sub>M</sub> = 40.8 Å <sup>2</sup> <i>L</i> = 31.75 Å <i>d/L</i> = 1.56
	57.75 VS 29.01 W 19.25 W	001 002 003	57.83 28.92 19.28					SmA: <i>T</i> = 170 °C <i>V</i> <sub>M</sub> = 1162 Å <sup>3</sup> <i>A</i> <sub>M</sub> = 40.2 Å <sup>2</sup> <i>L</i> = 38.77 Å <i>d/L</i> = 1.49
<b>6a</b>	50.04 VS	001	50.04					SmA: <i>T</i> = 210 °C <i>V</i> <sub>M</sub> = 1102 Å <sup>3</sup> <i>A</i> <sub>M</sub> = 44.0 Å <sup>2</sup> <i>L</i> = 30.63 Å <i>d/L</i> = 1.63
<b>7a</b>	46.92 VS 23.27 M 15.56 W	001 002 003	46.58 23.29 15.53					X: <i>T</i> = 170 °C <i>V</i> <sub>M</sub> = 1228 Å <sup>3</sup> <i>A</i> <sub>M</sub> = 52.8 Å <sup>2</sup> <i>L</i> = 38.40 Å
	51.77 VS 25.77 M 17.16 W	001 002 003	51.47 25.73 17.16					E: <i>T</i> = 200 °C <i>V</i> <sub>M</sub> = 1253 Å <sup>3</sup> <i>A</i> <sub>M</sub> = 48.6 Å <sup>2</sup> <i>L</i> = 38.40 Å <i>d/L</i> = 1.34
	59.46 VS 29.87 M 19.88 W	001 002 003	59.62 29.81 19.87					SmC: <i>T</i> = 205 °C <i>V</i> <sub>M</sub> = 1257 Å <sup>3</sup> <i>A</i> <sub>M</sub> = 42.2 Å <sup>2</sup> <i>L</i> = 38.40 Å
	67.48 VS 33.73 W 22.57 VW	001 002 003	67.56 33.78 22.52					SmA: <i>T</i> = 220 °C <i>V</i> <sub>M</sub> = 1269 Å <sup>3</sup> <i>A</i> <sub>M</sub> = 37.6 Å <sup>2</sup> <i>L</i> = 38.40 Å <i>d/L</i> = 1.76
<b>9a</b>	60.06 VS 30.02 M 20.02 S	001 002 003	60.00 30.00 20.00					X: <i>T</i> = 160 °C <i>V</i> <sub>M</sub> = 1373 Å <sup>3</sup> <i>A</i> <sub>M</sub> = 45.8 Å <sup>2</sup> <i>L</i> = 45.41 Å
	57.75 VS 29.15 M 19.37 S 4.65 M 4.16 W	001 002 003 110 200	58.19 29.10 19.40 4.65 4.16					E: <i>T</i> = 188 °C <i>V</i> <sub>M</sub> = 1399 Å <sup>3</sup> <i>A</i> <sub>M</sub> = 48.0 Å <sup>2</sup> <i>a</i> = 8.33 Å <i>b</i> = 5.60 Å <i>c</i> = 58.19 Å

**Table 2. Continued**

compound	<i>d</i> <sub>meas.</sub> / Å <sup>a</sup>	<i>I</i> <sup>b</sup>	<i>hkl</i> <sup>c</sup>	<i>d</i> <sub>calc.</sub> / Å <sup>a</sup>	parameters of smectic phase <sup>d–g</sup>
					<i>L</i> = 45.41 Å <i>d/L</i> = 1.28
<b>6b</b>	65.28 VS 32.63 M 21.60 M	001 002 003	65.12 32.56 21.71		SmC: <i>T</i> = 205 °C <i>V</i> <sub>M</sub> = 1415 Å <sup>3</sup> <i>A</i> <sub>M</sub> = 43.4 Å <sup>2</sup> <i>L</i> = 45.41 Å
	67.48 VS 33.54 M 22.41 M	001 002 003	67.26 33.63 22.42		SmA: <i>T</i> = 216 °C <i>V</i> <sub>M</sub> = 1425 Å <sup>3</sup> <i>A</i> <sub>M</sub> = 42.4 Å <sup>2</sup> <i>L</i> = 45.41 Å <i>d/L</i> = 1.48
<b>7b</b>	43.51 VS 21.76 VW	001 002	43.51 21.76		SmA: <i>T</i> = 105 °C <i>V</i> <sub>M</sub> = 1378 Å <sup>3</sup> <i>A</i> <sub>M</sub> = 63.4 Å <sup>2</sup> <i>L</i> = 30.63 Å <i>d/L</i> = 1.42
	61.28 VS 30.95 W	001 002	61.59 30.80		SmA: <i>T</i> = 125 °C <i>V</i> <sub>M</sub> = 1548 Å <sup>3</sup> <i>A</i> <sub>M</sub> = 50.2 Å <sup>2</sup> <i>L</i> = 38.40 Å <i>d/L</i> = 1.60
<b>9b</b>	53.62 VS 27.05 S	001 002	53.86 26.93		SmC: <i>T</i> = 120 °C <i>V</i> <sub>M</sub> = 1692 Å <sup>3</sup> <i>A</i> <sub>M</sub> = 62.8 Å <sup>2</sup> <i>L</i> = 45.41 Å
	54.60 VS 27.29 S	001 002	54.59 27.30		SmA: <i>T</i> = 135 °C <i>V</i> <sub>M</sub> = 1710 Å <sup>3</sup> <i>A</i> <sub>M</sub> = 62.6 Å <sup>2</sup> <i>L</i> = 45.41 Å <i>d/L</i> = 1.20
<b>3d</b>	50.89 VS 25.66 W	001 002	51.11 25.55		SmA: <i>T</i> = 140 °C <i>V</i> <sub>M</sub> = 2748 Å <sup>3</sup> <i>A</i> <sub>M</sub> = 53.8 Å <sup>2</sup> <i>L</i> = 31.75 Å <i>d/L</i> = 1.61
<b>5d</b>	61.28 VS 30.64 VW 20.42 W	001 002 003	61.28 30.64 20.43		SmC: <i>T</i> = 123 °C <i>V</i> <sub>M</sub> = 3014 Å <sup>3</sup> <i>A</i> <sub>M</sub> = 49.2 Å <sup>2</sup> <i>L</i> = 38.77 Å
	63.89 VS 31.94 VW 21.14 W	001 002 003	63.73 31.87 21.24		SmA: <i>T</i> = 140 °C <i>V</i> <sub>M</sub> = 3052 Å <sup>3</sup> <i>A</i> <sub>M</sub> = 47.9 Å <sup>2</sup> <i>L</i> = 38.77 Å <i>d/L</i> = 1.64
<b>6d</b>	45.49 VS	001	45.49		SmA: <i>T</i> = 225 °C <i>V</i> <sub>M</sub> = 3046 Å <sup>3</sup> <i>A</i> <sub>M</sub> = 67.0 Å <sup>2</sup> <i>L</i> = 30.63 Å <i>d/L</i> = 1.49
<b>7d</b>	63.89 VS	001	63.89		SmA: <i>T</i> = 195 °C <i>V</i> <sub>M</sub> = 3302 Å <sup>3</sup> <i>A</i> <sub>M</sub> = 51.7 Å <sup>2</sup> <i>L</i> = 38.40 Å <i>d/L</i> = 1.66
<b>8d</b>	48.82 VS	001	48.82		SmA: <i>T</i> = 210 °C <i>V</i> <sub>M</sub> = 3335 Å <sup>3</sup> <i>A</i> <sub>M</sub> = 68.3 Å <sup>2</sup> <i>L</i> = 38.23 Å <i>d/L</i> = 1.28

Table 2. Continued

compound	$d_{\text{meas.}}/\text{\AA}^a$	$I^b$	$hkl^c$	$d_{\text{calc.}}/\text{\AA}^a$	parameters of smectic phase <sup>d-g</sup>
<b>9d</b>	57.75	VS	001	57.70	SmF/SmI: $T = 170 \text{ }^\circ\text{C}$
	28.59	W	002	28.85	$V_M = 3557 \text{ \AA}^3$
	19.25	S	003	19.23	$A_M = 61.7 \text{ \AA}^2$
	5.48	VW	110	5.48	$L = 45.41 \text{ \AA}$
	4.53	VW	$h_{\text{hexagonal}}$		
	3.91	VW	200	3.87	
	3.49	VW	210	3.46	
	61.28	VS	001	61.92	SmC: $T = 210 \text{ }^\circ\text{C}$
	31.27	VW	002	30.96	$V_M = 3653 \text{ \AA}^3$
	20.85	W	003	20.64	$A_M = 59.0 \text{ \AA}^2$
					$L = 45.41 \text{ \AA}$
	63.89	VS	001	63.89	SmA: $T = 230 \text{ }^\circ\text{C}$ $V_M = 3701 \text{ \AA}^3$ $A_M = 57.9 \text{ \AA}^2$ $L = 45.41 \text{ \AA}$ $d/L = 1.41$

<sup>a</sup>  $d_{\text{meas.}}$  and  $d_{\text{calc.}}$  are the measured and calculated diffraction spacings, respectively. <sup>b</sup>  $I$  is the intensity of the reflections: VS, very strong; S, strong; M, medium; W, weak; VW, very weak; br, broad reflection. <sup>c</sup>  $hkl$  are the Miller indices of the reflections.  $h_{\text{hexagonal}}$  denotes the wide-angle reflection that was indexed as the (10) reflection on a two-dimensional hexagonal lattice. <sup>d</sup>  $T$  is the temperature at which the X-ray diffractogram was recorded. <sup>e</sup>  $V_M$  is the molecular volume,  $A_M$  is the molecular area (for the bromide and bis(trifluoromethylsulfonyl)imide salts,  $A_M = 2V_M/d$ ; for the tetrabromouranyl salts,  $A_M = V_M/d$ ). <sup>f</sup>  $a$ ,  $b$ , and  $c$  are the dimensions of the orthorhombic unit cell in the crystal smectic E phase. Because indexation of the powder X-ray diffractogram of **7a** at 200 °C was not straightforward, no values are given for  $a$ ,  $b$ , and  $c$ . <sup>g</sup>  $L$  is the calculated length of the relevant pyrrolidinium cation in its most extended conformation (estimated with Chem3D; the structure of the pyrrolidinium cation was energy-minimized via an MM2 calculation within Chem3D). <sup>h</sup> Not detected because of overlap with the diffraction signal produced by the covering foil, used in the experimental setup (this signal occurs at  $2\theta = 5.7\text{--}7.6 \text{ \AA}^{-1}$ ). <sup>i</sup> This reflection partly overlaps with the (009) reflection. <sup>j</sup> During the temperature scan of the X-ray diffraction measurement, the SmA phase was observed at somewhat lower temperatures than indicated by DSC (Table 1). This might point to a slight decomposition of the sample at high temperatures.

calculated length of the cation in its most extended conformation) was found to decrease with increasing spacer length, and increase with increasing terminal chain length (except for the SmA phases shown by compounds **3d** and **5d**, where  $d/L$  is almost equal for both phases).

In the following sections, the X-ray diffraction data will be discussed more thoroughly per compound type.

(a) *Mesophase Structure of the Bromide Salts.* (i) *SmA Phases.* In Figure 4, a structural model for the SmA phase shown by compound **3a** is proposed. The smectic layer interfaces are formed by ionic sublayers. Each ionic sublayer consists of two monolayers containing the ionic head groups (with alternating positive and negative charges). The ionic sublayers are separated from each other by sublayers containing flexible alkyl spacers, biphenyl moieties, and terminal alkyl chains. A similar “antiparallel” arrangement, allowing for a close proximity of the cationic head groups and the bromide anions, was also suggested for the SmA phases shown by imidazolium ionic liquid crystals with pendant cholesterol groups.<sup>12</sup> At 180 °C, the layer thickness  $d$  equals 49.63 Å (Table 2). This value is about 1.56 times the calculated length  $L$  of the cation in its most extended conformation. For the proposed molecular arrangement, the molecular area  $A_M$  occupied by an ionic cluster (i.e., a dimer of two antiparallel cations and two bromide anions) can be estimated using the relation  $A_M = 2V_M/d$ , where  $V_M$  is the molecular volume (estimated as  $V_M = (M/0.6022)f$ , where  $M$  is the

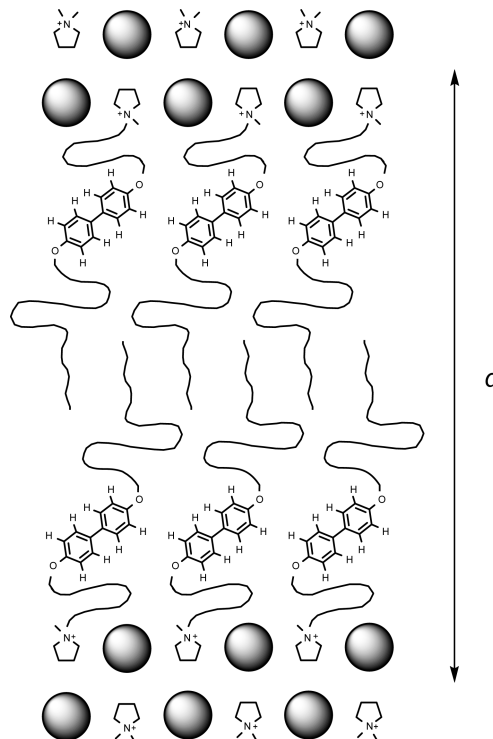


**Figure 4.** Structural model for the de Vries type SmA phase exhibited by compound **3a**. Bromide anions are represented by gray spheres, but cations are not displayed in space-filling mode. The smectic layer thickness is indicated by  $d$  (at 180 °C:  $d = 49.63 \text{ \AA}$ ,  $A_M = 40.8 \text{ \AA}^2$  (Table 2)). The thickness of the ionic sublayer and the lateral separation of the cations and anions were estimated from the results obtained in our previous report on pyrrolidinium ionic liquid crystals.<sup>5</sup>

molecular mass ( $\text{g mol}^{-1}$ ) and  $f$  is a temperature correcting factor ( $f = 0.9813 + 7.474 \times 10^{-4}T$ ;  $T$  in °C)).<sup>12</sup> At 180 °C, this calculation gives a value of  $A_M \approx 40.8 \text{ \AA}^2$ . In principle, assuming a parallel arrangement of the mesogenic groups perpendicular to the smectic layers, the calculated  $A_M$  value would correspond to a lateral packing area per mesogenic group of about 20.4 Å<sup>2</sup>, which is slightly smaller than typical figures for the cross section of rodlike mesogenic groups (e.g., 22–24 Å<sup>2</sup> for a cyanobiphenyl group).<sup>55</sup> However, this simple and most obvious molecular packing does not suit space-filling requirements: since the measured smectic layer thickness is so large, the combined length of spacer and terminal alkyl chain is not large enough to fill all empty space, as indicated in Figure S14 in the Supporting Information. Therefore, an alternative arrangement is proposed, wherein the spacers are highly folded and the rigid mesogenic groups are tilted (with respect to the layer normal) within the smectic layers (Figure 4). In this model, the complete molecular area occupied by an ionic head group (a pyrrolidinium ring and a bromide anion) is covered by a single tilted aromatic system. As such, the SmA phase exhibited by compound **3a** is a *de Vries type* SmA phase. In *de Vries type* SmA phases, the molecules are tilted (as in the SmC phase) but without any correlation in the direction of tilt.<sup>56–58</sup> The resulting phase is therefore optically uniaxial. Assuming a cross section of 24 Å<sup>2</sup> for the biphenyl moieties, the tilt angle  $\theta_t$  (between the layer normal and the long molecular

(55) Cardinaels, T.; Driesen, K.; Parac-Vogt, T. N.; Heinrich, B.; Bourgogne, C.; Guillon, D.; Donnio, B.; Binnemans, K. *Chem. Mater.* **2005**, *17*, 6589–6598.

(56) de Vries, A. *Mol. Cryst. Liq. Cryst.* **1977**, *41*, 27–31.

(57) de Vries, A.; Ekachai, A.; Spielberg, N. *Mol. Cryst. Liq. Cryst.* **1979**, *49*, 143–152.

(58) de Vries, A. *J. Chem. Phys.* **1979**, *71*, 25–31.

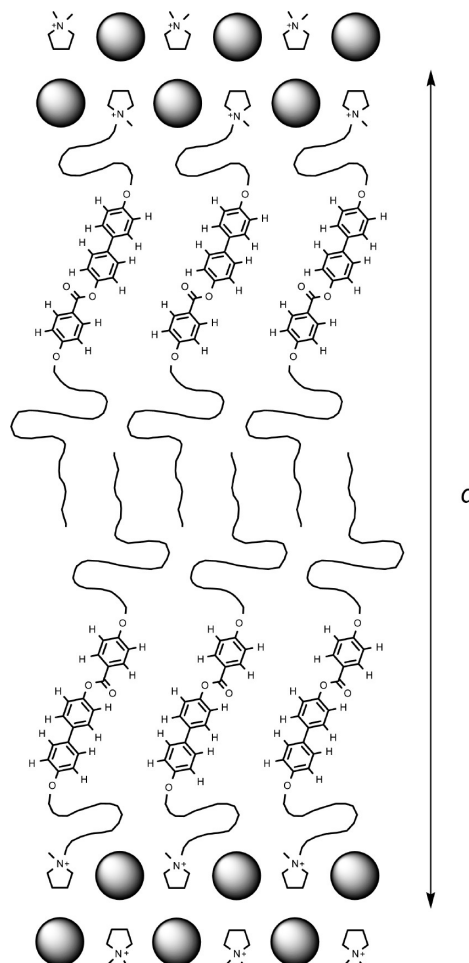


**Figure 5.** Structural model for the de Vries type SmA phase exhibited by compound **7a**. The smectic layer thickness is indicated by  $d$  (at 220 °C:  $d = 67.56 \text{ \AA}$ ,  $A_M = 37.6 \text{ \AA}^2$  (Table 2)).

axes of the rigid aromatic parts) will be approximately equal to  $\cos^{-1}(24/40.8) \approx 54^\circ$ . From Figure 4, it is clear that the smectic layer formation is mainly due to the strong electrical forces between the cations and anions. Electrical interactions between molecules are indeed known to be stronger than van der Waals interactions.<sup>59</sup> Nevertheless, the terminal alkyl chains interdigitate and interact via van der Waals forces; they form a separate sublayer within the smectic layers. Since the cross-sectional area of one fully stretched aliphatic chain equals about 23.8 Å<sup>2</sup> at 180 °C, the two terminal alkyl chains of an ionic cluster are not fully interdigitated.<sup>60</sup> Figure 4 displays a possible conformation of highly folded terminal chains that form the aliphatic continuum in the center of a smectic layer.

The question remains why the smectic layer thickness  $d$  and thus the ratio  $d/L$  are so large and why the molecules adopt such unusual conformation. A full interdigitation of the (spacer—perpendicularly oriented rigid mesogenic group—terminal alkyl chain) combinations, to completely counterbalance the molecular area of the ionic head groups, would be more logical. The relatively long terminal decyl chain is believed to be of importance in this aspect. For the SmA phases shown by halide salts of pyridinium cations with a mesogenic 4'-methoxybiphenyl-4-yloxy group,  $d/L$  ratios around unity were reported

(with  $L$  representing the calculated length of both the cation and the anion in the prolongation of the cation),<sup>14</sup> for the SmA phase shown by *N*-[10-(4'-propyloxybiphenyl-4-yloxy)decyl]pyridinium bromide,  $d/L$  was found to be 1.15 (with  $L$  representing the calculated length of only the cation; by including the bromide anion,  $d/L \approx 1$ ).<sup>16</sup> On the other hand, much higher  $d/L$  values of 1.50 and 1.63 were found for the SmA phases shown by *N*-[10-(4'-decyloxybiphenyl-4-yloxy)decyl]-4-ethylpyridinium bromide (**10**) and *N*-[10-(4'-decyloxybiphenyl-4-yloxy)decyl]-2-ethylpyridinium bromide (**11**), respectively.<sup>16</sup> It appears that, only for relatively long terminal chain lengths, the van der Waals interactions between the aliphatic chains are strong enough to induce a microphase separation into a separate aliphatic sublayer. This results in increased  $d$  and  $d/L$  values. In ref 16, a partly interdigitated head-to-head bilayer structure with nontilted biphenyl groups was proposed for the SmA phases of **10** and **11**. However, this model clearly does not suit space-filling requirements. Without a full interdigitation (discarded because  $d \gg L$ ), the molecular area of the ionic head groups cannot be counterbalanced by a single, nontilted biphenyl group; it cannot fill space efficiently on its own. Of course, it should be mentioned that the molecular area of the ionic head group is highly dependent on the choice of the halide anion. Interestingly, tilting of the biphenyl moieties in the SmA phase of compound **3a** occurs without the aid of attractive Coulombic interactions between a partial positive charge on one end of a calamitic core and a partial negative charge on the other end of the calamitic core next to it in the smectic layer, like in the case of dipolar 4,4'-oxynitrostilbene cores.<sup>61</sup>

For the same reasons as outlined above, the SmA phase shown by compound **5a** must be of the de Vries type as well. A similar model as the one shown in Figure 4 can be drawn.

The same reasoning applies to the SmA phase shown by compound **7a**, which is the analogue of compound **3a** with an extended mesogenic group. The  $d/L$  ratio at 220 °C was found to be 1.76, while  $A_M$  equals only 37.6 Å<sup>2</sup>. Clearly, the available molecular area in the smectic planes, determined by the ionic head groups, is too small to accommodate two mesogenic groups next to each other. On the other hand,  $A_M$  is slightly too large to be occupied by a single, nontilted mesogenic unit; although no literature values could be found for the lateral packing area of the three-ring aromatic group, we estimated this area to be about 1.5 times the cross section of a classical, truly rodlike mesogenic group, that is, about  $1.5 \times 24 \text{ \AA}^2 = 36 \text{ \AA}^2$  (this seems logical, as the cross section of the 4-alkoxybenzoate part overlaps for about 50% with the rodlike biphenyl part). Due to space-filling requirements, a parallel arrangement of perpendicularly oriented mesogenic groups wherein the transverse area of one aromatic system partly overlaps with that of the other aromatic system of the ionic cluster (which is theoretically possible because of the large smectic layer thickness  $d$ ) is discarded. Therefore, we propose a similar molecular packing in the SmA phase shown by compound **7a** as the one depicted in Figure 4 for compound **3a** (Figure 5). The SmA phase is of the de Vries type. Because of the smaller value found for  $A_M$  and the longer aromatic system in comparison to compound **3a**, the tilt angle of the three-ring mesogenic groups in the SmA phase of **7a** will be much smaller than the tilt angle of the biphenyl moieties in the SmA phase of **3a**. Indeed, the tilt angle will be approximately equal to  $\cos^{-1}(36/37.6) \approx 17^\circ$ .

Interestingly, for the SmA phase shown by compound **6a**, a  $d/L$  ratio of 1.63 was found at 210 °C. As mentioned above, for

(59) Israelachvili, J. N. *Intermolecular and Surface Forces*; Academic Press: London, 1992.

(60) Marcos, M.; Giménez, R.; Serrano, J. L.; Donnio, B.; Heinrich, B.; Guillon, D. *Chem.—Eur. J.* **2001**, *7*, 1006–1013.

(61) Tittarelli, F.; Masson, P.; Skoulios, A. *Liq. Cryst.* **1997**, *22*, 721–726.

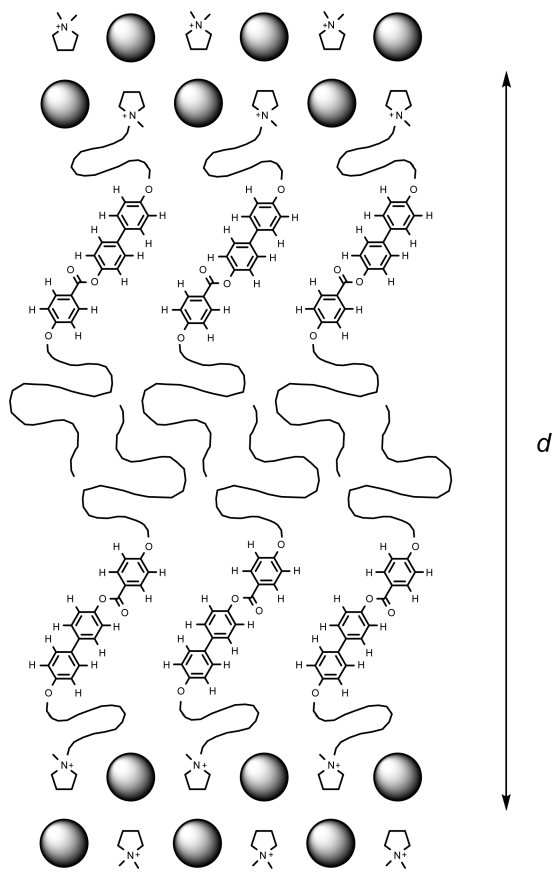


**Figure 6.** Structural model for the SmC phase exhibited by compound **7a**. The smectic layer thickness is indicated by  $d$  (at 205 °C:  $d = 59.62 \text{ \AA}$ ,  $A_M = 42.2 \text{ \AA}^2$  (Table 2)).

pyridinium ionic liquid crystals with pendant biphenyl moieties bearing short terminal alkyl chains ( $C_1$  or  $C_3$ ), a full interdigititation of the cations in an ionic cluster was observed ( $d/L$  values close to unity). This is not the case for **6a**, which contains a short terminal alkyl chain ( $C_4$ ), but a three-ring mesogenic group instead of a biphenyl moiety. We suggest a similar molecular packing in the SmA phase of **6a** as the one depicted in Figure 5, but with a somewhat larger tilt angle of the aromatic systems ( $A_M \approx 44.0 \text{ \AA}^2$  at 210 °C). The terminal alkyl chains will form an aliphatic continuum in the center of the smectic layers.

Finally, based on the parameters  $d$ ,  $d/L$ , and  $A_M$ , it was found that the SmA phase shown by compound **9a** is also of the de Vries type. Since the calculated  $A_M$  value is close to that found for **6a**, the average tilt angle of the aromatic systems will be more or less the same in both SmA phases. Thus, the tilt angle seems to be larger when the alkyl spacer and the terminal alkyl chain have the same length.

(ii) *SmC Phases.* For compound **7a**, the molecular area occupied by an ionic cluster is larger in the SmC phase than in the SmA phase ( $42.2 \text{ \AA}^2$  versus  $37.6 \text{ \AA}^2$ ). Thus, the rigid cores are tilted to a greater extent than in the SmA phase (see below). As a consequence, the smectic layer thickness is smaller and the terminal aliphatic chains are more interdigitated. A model is proposed in Figure 6. The transition from the SmC phase of **7a** to its SmA phase is thus characterized by a decrease in the tilt angle as well as the loss of correlation in the direction of tilt.

The tilt angle  $\theta_t$  could be estimated by plotting the layer thickness  $d$  in the different mesophases as a function of the temperature (see the Supporting Information, Figure S13).

Indeed, it was found that, at least for *N*-(4'-*n*-butyloxybenzylidene)-4-*n*-heptylaniline, it is possible to calculate the tilt angle at a certain temperature  $T_x$  by extrapolating the SmA layer thickness,  $d_{\text{SmA}}$ , into the SmC phase (using the equation of a linear fit of the SmA layer thickness data) and by using the relation  $\theta_t \approx \cos^{-1}(d_{\text{SmC}}(T_x)/d_{\text{SmA}}(T_x))$ .<sup>48</sup> In this way, a value of  $\theta_t \approx 31^\circ$  was obtained for the SmC phase of **7a** at 205 °C. On the other hand, again assuming a cross section of  $36 \text{ \AA}^2$  for the mesogenic groups, the tilt angle can also be calculated from  $\cos^{-1}(36/42.2) \approx 31^\circ$ . As such, the two methods of calculation yield exactly the same result, supporting the proposed model.

Similar arguments apply to the SmC phase shown by compound **9a**. In this case, however, the structural parameters  $d$  and  $A_M$  found for the SmC phase and the SmA phase do not differ much, indicating an analogous molecular packing in both phases. The transition from the SmC phase to the SmA phase is again characterized by a loss of correlation in the direction of tilt.

(iii) *E Phases.* As mentioned above, the X-ray diffractogram of compound **3a** at 150 °C displays two signals in the wide-angle region, centered at about 4.73 and 3.74 Å. These reflections, albeit rather weak, indicate a two-dimensional ordering of the molecules within the smectic layers, and were indexed as the (110) and (200) reflections from a two-dimensional centered rectangular lattice. This indexation allowed us to calculate the unit cell parameters  $a$  and  $b$ :  $a = 7.48 \text{ \AA}$ ,  $b = 6.09 \text{ \AA}$ . Consequently, the area of the base of the rectangular lattice unit cell, which corresponds to the molecular area covered by the ionic head groups of an ionic cluster, equals  $45.6 \text{ \AA}^2$ . This value corresponds quite well to the calculated molecular area  $A_M$  ( $47.2 \text{ \AA}^2$ ). It is somewhat larger than  $A_M$  obtained for the SmA phase of **3a**. Similar values were found for the E phase of *N*-alkylpyridinium halides  $\omega$ -substituted with a 4'-methoxybiphenyl-4-yloxy group.<sup>14</sup> Although a lateral packing area of  $22.8 \text{ \AA}^2$  per nontilted mesogenic biphenyl group is commonly observed in liquid crystal phases,<sup>14,55</sup> and although the smectic layer thickness in the E phase is smaller than the SmA layer thickness, the biphenyl groups are assumed to be tilted, like in the higher-temperature de Vries type SmA phase (tilt angle approximately equal to  $\cos^{-1}(24/45.6) \approx 58^\circ$ ) (Figure 7). Indeed, a parallel arrangement of perpendicularly oriented mesogenic groups does not suit space-filling requirements once more, because the layer thickness is still rather large as compared to the length of the cations. Probably the tilt of the aromatic systems is induced once again by the van der Waals interactions between the long terminal alkyl chains. The molecular area  $A_M$  is large enough to allow an almost complete interdigititation of the chains (the cross-sectional area of one fully stretched aliphatic chain equals about  $23.3 \text{ \AA}^2$  at 150 °C<sup>60</sup>). The top view of the two-dimensional rectangular lattice illustrates the herringbone molecular packing which is typical for the E phase.<sup>47,48</sup>

It should be noted that, in addition to the wide-angle peaks mentioned above, some more very weak diffraction signals were observed in the wide-angle region. These peaks could be indexed as the (114), (202), (204), and (206) reflections of an orthorhombic lattice with unit cell parameters  $a = 7.48 \text{ \AA}$ ,  $b = 6.09 \text{ \AA}$ , and  $c = d = 42.15 \text{ \AA}$ , supporting the designation as a crystal smectic E phase. The phase is thus characterized by a weak interlayer coupling.

Like in the case of **3a**, the X-ray diffractograms of compounds **5a** (at 145 °C) and **9a** (at 188 °C) displayed two signals in the wide-angle region, centered at about 4.62 and 4.12 Å, and at about 4.65 and 4.16 Å, respectively. These were also indexed as the (110) and (200) reflections of a two-dimensional rectangular lattice. The unit cell parameters  $a$  and  $b$  equal 8.24 and 5.58 Å in the case of **5a**, and 8.33 and 5.60 Å in the case of **9a** respectively.

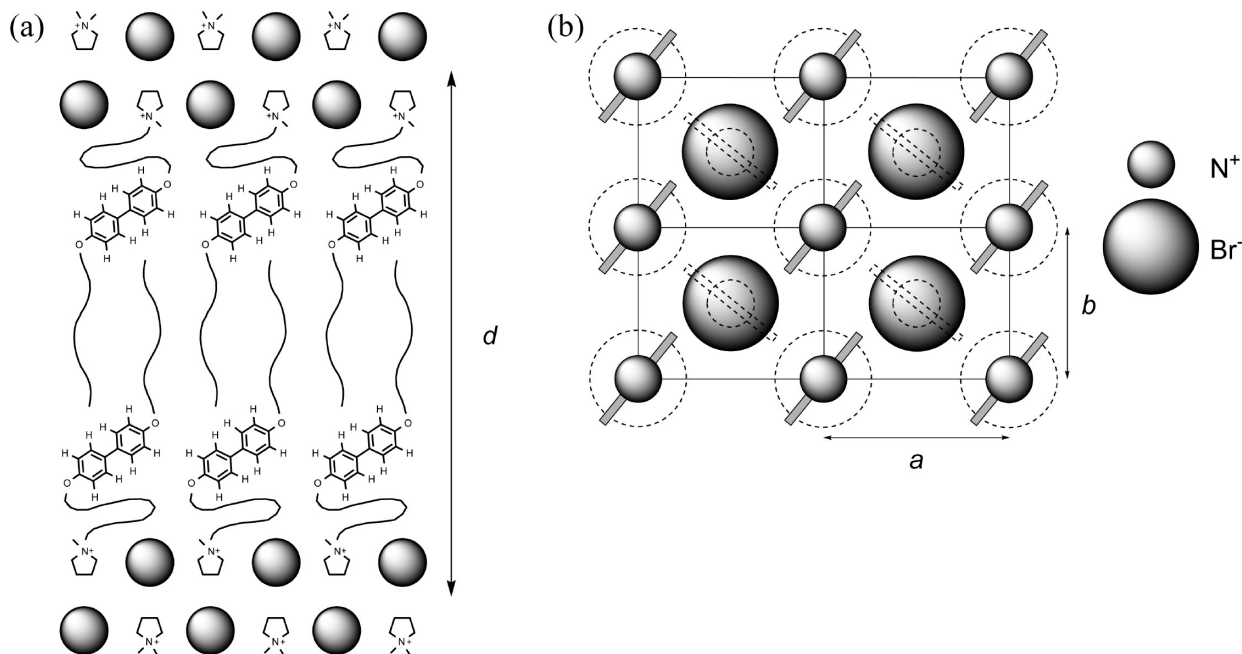


**Figure 7.** Structural model for the crystal smectic E phase exhibited by compound **3a**.<sup>14</sup> (a) Side view. The smectic layer thickness is indicated by  $d$  (at 150 °C;  $d = 42.15 \text{ \AA}$ ,  $A_M = 47.2 \text{ \AA}^2$  (Table 2)). The pyrrolidinium rings are in fact tilted out of the plane of the paper, as illustrated in (b). (b) Top view of the two-dimensional rectangular lattice. The pyrrolidinium rings are schematically represented as rectangles (although the pyrrolidinium ring is not entirely planar, with the nitrogen atom sitting above the plane of the four-ring carbon atoms in the envelope conformation), and the substituents on the pyrrolidinium nitrogen atoms are omitted for clarity. The dimensions of a unit cell of the two-dimensional rectangular lattice are indicated by  $a$  and  $b$ .

Consequently, the areas  $a \times b$  are similar to the value obtained for compound **3a**. Similar molecular packings as the one depicted in Figure 7 are proposed. Also, for both **5a** and **9a**, some more very weak wide-angle peaks that indicate a weak interlayer coupling were observed. The powder X-ray diffractogram of compound **7a** at 200 °C also showed multiple wide-angle peaks, but indexation was not straightforward. The phase was designated as a crystal smectic E phase on the basis of the observed texture, which resembled the textures of the E phases shown by compounds **3a**, **5a**, and **9a** (see above).

(b) *Mesophase Structure of the Bis(trifluoromethylsulfonyl)imide Salts.* (i) *SmA Phases.* When comparing the structural parameters  $d$ ,  $d/L$ , and  $A_M$  of the SmA phases shown by compounds **6b**, **7b**, and **9b** with those of the SmA phases shown by the corresponding bromide salts **6a**, **7a**, and **9a**, it is clear that replacement of the bromide anion by the larger bis(trifluoromethylsulfonyl)imide anion leads to lower  $d$  and  $d/L$  values and higher  $A_M$  values. The higher  $A_M$  values correspond to the obviously larger molecular area occupied by an ionic cluster (a dimer of two cations and two bis(trifluoromethylsulfonyl)imide anions), assuming a similar “antiparallel” arrangement as proposed for the bromide salts (such arrangement was also suggested for the SmA phase of an imidazolium bis(trifluoromethylsulfonyl)imide salt<sup>12</sup>). This larger molecular area needs to be compensated by a larger tilt of the aromatic systems in the de Vries type SmA phases. At the same time, the spacers are highly folded. This rather unfavorable conformation is probably the reason for the small mesophase stability ranges of compounds **6b**, **7b**, and **9b**. On the basis of the found structural parameters, a classical SmA phase containing nontilted mesogenic groups is discarded: although the  $d/L$  ratios are smaller in comparison to the bromide salts, the measured smectic layer thicknesses are still too large for a full interdigitation of the cations of an ionic cluster. Moreover, both spacers and terminal alkyl chains need to be highly folded, since the cross-sectional area of a single fully

stretched aliphatic chain equals about 22.8  $\text{\AA}^2$  at 120 °C,<sup>60</sup> while the  $A_M$  values found are 63.4, 50.2, and 62.6  $\text{\AA}^2$  for **6b** (at 105 °C), **7b** (at 125 °C), and **9b** (at 135 °C), respectively. Therefore, the actual length of the cations within the smectic layers will be shorter than  $L$  anyway.

(ii) *SmC Phase (Compound 9b).* The structural parameters  $d$  and  $A_M$  found for the SmC phase and the SmA phase shown by compound **9b** do not differ much. This indicates an analogous molecular packing in both phases. The transition from the SmC phase of **9b** to its SmA phase is characterized by a loss of correlation in the direction of tilt.

(c) *Mesophase Structure of the Tetrabromouranyl Salts.* (i) *SmA Phases.* In Figure 8, a structural model for the SmA phase shown by compound **3d** is proposed. Each molecule contains two cations because of the double negative charge of  $[UO_2Br_4]^{2-}$ . The smectic layer interfaces are now formed by monolayers of  $[UO_2Br_4]^{2-}$  anions, with the cationic head groups situated above and below those monolayers. When comparing to the packing in the crystal structure of compound **6d** (Figure 2), this structure is reminiscent of the crystalline solid state. The salt molecules are not forced to self-assemble into ionic *double* layers, as in the case of the *N*-alkyl-*N*-methylpyrrolidinium tetrabromouranyl salts,<sup>5</sup> since the rigid mesogenic groups, in contrast to simple alkyl chains, can tilt to compensate for the large ionic moiety. The complete sublayer containing cations and anions is expected to be thicker than the combination of the two ionic monolayers in the SmA phase of compound **3a**. On the other hand, the layer thickness  $d$  equals 51.11  $\text{\AA}$  at 140 °C, which is only slightly larger than the value found for **3a**. The molecular area  $A_M$ , however, obtained from  $V_M/d$  is clearly larger for the uranyl complex than for the bromide salt (53.8  $\text{\AA}^2$  versus 40.8  $\text{\AA}^2$ ), because of the size difference of the anions. As in the case of **3a**, it is unlikely that the aromatic systems are not tilted within the smectic layers, as this packing does not suit space-filling requirements because of the large  $d/L$  ratio; moreover, assuming a

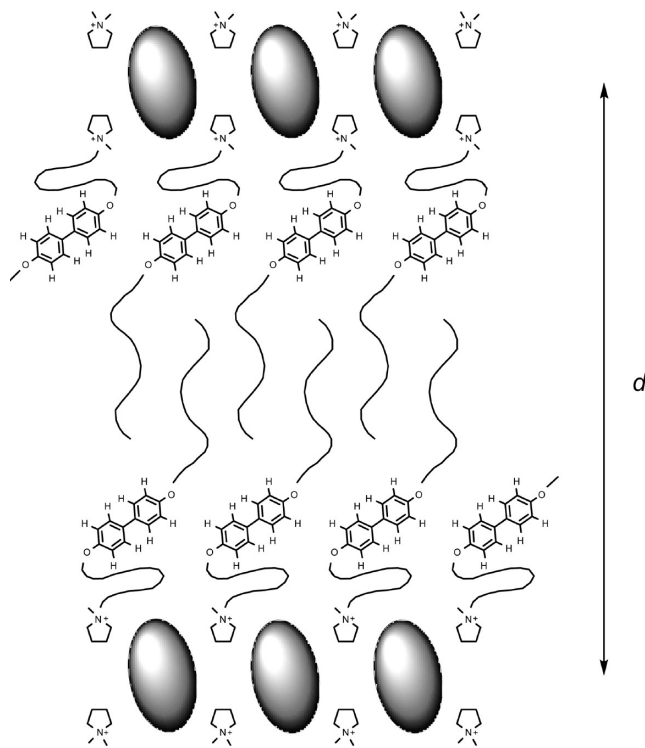


**Figure 8.** Structural model for the de Vries type SmA phase exhibited by compound **3d**. Tetrabromouranyl anions are represented by gray ellipsoids (these anions are distorted octahedrons, as the interatomic U–Br distance is larger than the U–O distance), but cations are not displayed in space-filling mode. The smectic layer thickness is indicated by  $d$  (at  $140\text{ }^{\circ}\text{C}$ :  $d = 51.11\text{ \AA}$ ,  $A_M = 53.8\text{ \AA}^2$  (Table 2)). The orientation of the ellipsoid tetrabromouranyl anions with respect to the pyrrolidinium rings was estimated on the basis of the crystal structure of compound **6d**.

parallel arrangement of perpendicularly oriented mesogenic groups, the calculated  $A_M$  value would correspond to a lateral packing area per mesogenic group of about  $27\text{ \AA}^2$ , which is larger than the typical cross section of rodlike biphenyl moieties (see above). Therefore, we suggest that the SmA phase is of the de Vries type. The terminal alkyl chains are fully interdigitated and folded (the cross-sectional area of a single fully stretched aliphatic chain equals about  $23.1\text{ \AA}^2$  at  $140\text{ }^{\circ}\text{C}$ <sup>60</sup>).

Similar models as the one depicted in Figure 8 can be drawn for the SmA phases shown by the other tetrabromouranyl salts, compounds **5d** and **6d–9d**. Differences in tilt angle occur.

(ii) *SmC Phases.* Based on the structural parameters  $d$  and  $A_M$ , it appears that the transition from the SmC phase to the SmA phase is characterized by a decrease in the tilt angle as well as the loss of correlation in the direction of tilt for both compounds **5d** and **9d**. However, the molecular packing in the SmC phase resembles that in the SmA phase. This was also found for bromide salt **7a** (see above).

(iii) *SmF/SmI Phase (Compound 9d).* In the wide-angle region of the diffractogram of compound **9d** at  $170\text{ }^{\circ}\text{C}$ , a weak reflection (superimposed on the broad halo associated with the lateral short-range order of the molten aliphatic chains) was observed at  $4.53\text{ \AA}$ . This reflection was indexed on a two-dimensional hexagonal lattice as the (10) peak. The phase is characterized by a pseudo-hexagonal packing of the tilted rigid cores within the smectic layers, with a lateral separation between the cores of about  $(2/3)^{1/2} \times 4.53\text{ \AA} = 5.23\text{ \AA}$ . The calculated molecular area,  $61.7\text{ \AA}^2$ , corresponds to a tilt angle of about  $\cos^{-1}(36/61.7) \approx 54^\circ$ . Interestingly, Tittarelli et al. noted that rods

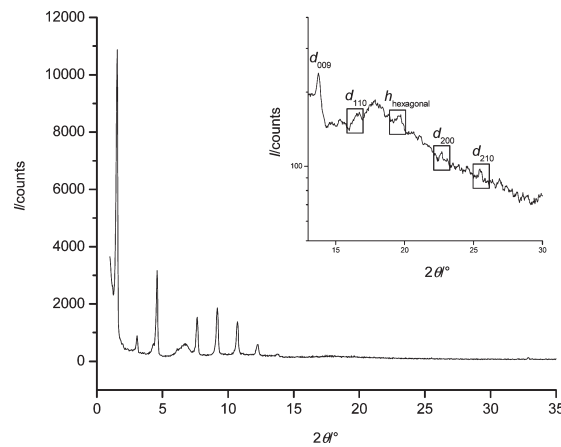


**Figure 9.** X-ray diffractogram of **9d** in the SmF/SmI phase at  $170\text{ }^{\circ}\text{C}$ , represented as the scattering intensity (in counts) versus the scattering angle,  $2\theta$  (the broad diffraction signal centered at  $20 \approx 6.5^\circ$  is due to the covering foil used in the experimental setup). Inset: magnification of the medium- and wide-angle region of the diffractogram, represented as the logarithm of the scattering intensity (in counts) versus the scattering angle,  $2\theta$ ;  $h_{\text{hexagonal}}$  denotes the reflection associated with the lateral hexagonal packing of the rigid aromatic cores; the broad diffraction signal centered at about  $4.8\text{ \AA}$  is associated with the lateral short-range order of the disordered (molten) aliphatic chains.

placed at the nodes of a two-dimensional square network and leaning over the diagonals of the square network over an angle of exactly  $54.7^\circ$  with respect to the plane normal are arranged laterally in a hexagonal fashion.<sup>61</sup> As such, the calculated tilt angle for the SmF/SmI phase of **9d** suggests that the two-dimensional intralayer packing of the tetrabromouranyl anions and pyrrolidinium head groups is locally tetragonal (with a  $[\text{UO}_2\text{Br}_4]^{2-}$  dianion in the center of a cube or cuboid and the cations on the eight vertices), which allows the tilted mesogenic moieties to be laterally packed according to a hexagonal lattice. This is supported by the observation of some additional very weak wide-angle signals that could be indexed as the (110), (200), and (210) reflections of a square lattice (reciprocal spacings of the reflections in the characteristic ratios  $1:2^{1/2}:(5^{1/2}/2^{1/2})$ ) (Figure 9). The unit cell parameter,  $a$ , of the square lattice, as obtained from  $d_{110}$ , equals about  $7.6\text{ \AA}$ . This value is in good agreement with  $A_M^{1/2} = (61.7\text{ \AA}^2)^{1/2} \approx 7.85\text{ \AA}$ . Of course, since there exists only short-range positional order within the smectic layers for SmF and SmI phases, the tetragonal intralayer lattice and consequently the hexagonal packing are not very well developed. This explains the weak and rather broad wide-angle signals. In conclusion, the changes in the molecular packing of compound **9d** in going from the SmF/SmI phase over the SmC phase toward the SmA phase can be summarized as follows: at the SmF/SmI-SmC transition, the tilt angle decreases slightly and the lateral hexagonal ordering of the mesogenic groups ceases to exist; at the SmC-SmA transition, the tilt angle decreases somewhat more and the correlation in the direction of tilt is lost.

Finally, we would like to emphasize that no orthogonal SmB phases or crystal smectic B phases, which are characterized by a two-dimensional hexagonal packing of nontilted molecules within the smectic layers, were observed for the reported pyrrolidinium ionic liquid crystals. The tilted SmF/SmI phase shown by compound **9d**, which was discussed above, is characterized by a lateral hexagonal packing of the calamitic cores, but the ionic head groups within the ionic sublayers are locally arranged according to a square network. This is not a coincidence: ordering of ions in a square two-dimensional network, with cations and

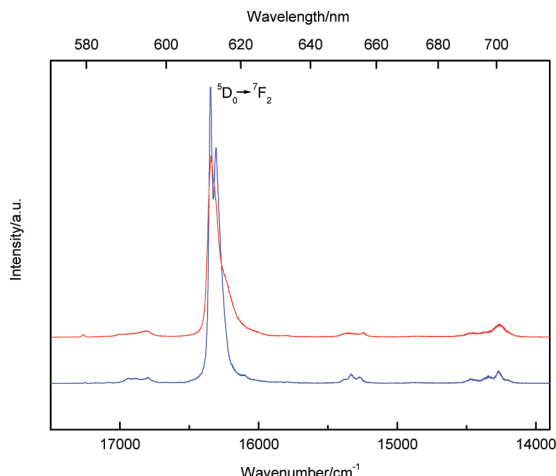


**Figure 10.** Photoluminescence spectra of the pure europium(III) complex **7c** (blue line) and a mixture of bromide salt **7a** and europium(III) complex **7c** in a 99:1 molar ratio (red line) in the solid state at room temperature (excitation wavelength: 370 nm).

anions at the corners and centers (or, for dianions like  $[UO_2Br_4]^{2-}$ , with an anion in the center of a cube or cuboid and the cations on the eight vertices), allows a strict alternation of positive and negative charges. When both the cations and the anions are relatively large and/or anisometric (and assuming that they do not form ion pairs), a hexagonal two-dimensional ordering of the ions seems to be less favorable. For ionic liquid crystals resembling the pyrrolidinium salts presented here, only very few examples of a SmB phase have been reported.<sup>14,62,63</sup> Bazuin et al. described a SmB phase exhibited by *N*-hexadecyl-4-cyanopyridinium iodide, but this phase has an unusual partial bilayer honeycomb structure that is associated with interactions between the polar cyano substituents.<sup>64</sup>

**Luminescence Properties.** Since the pure europium(III) compound **7c** was not liquid-crystalline, it was mixed with the corresponding mesomorphic bromide salt **7a** in different molar ratios to obtain liquid-crystalline mixtures. The homogeneous mixtures showed an intense red photoluminescence (shown in Figure 10 for a mixture of **7a** and **7c** in a 99:1 molar ratio). The question may arise whether the first coordination sphere of the  $[Eu(tta)_4]^-$  anion remains intact in the presence of the bromide salt. Therefore, the luminescence spectrum of the pure europium(III) complex **7c** was compared with the spectra of the different bromide-containing mixtures. In Figure 10, the luminescence spectra of the pure europium(III) complex and the 99:1 mixture are given. The spectrum of **7c** is dominated by the very intense hypersensitive  $^5D_0 \rightarrow ^7F_2$  transition with a maximum at 612 nm. The luminescence decay curve was found to be biexponential, with the two lifetimes being  $\tau_1 = 580 \mu s$  (57%) and  $\tau_2 = 316 \mu s$  (43%). The luminescence spectrum of the 99:1 mixture looks similar to that of the pure complex **7c**, although there are some minor differences in the crystal-field fine structure. This is an indication that the first coordination sphere remains more or less intact. Replacement of 2-thenoyltrifluoroacetone ligands by bromide ligands would result in major changes in the intensity of the hypersensitive  $^5D_0 \rightarrow ^7F_2$  transition relative to the other nonhypersensitive transitions, in particular

the  $^5D_0 \rightarrow ^7F_1$  transition. However, it was found that the luminescence decay times were significantly shorter for the 99:1 mixture:  $\tau_1 = 398 \mu s$  (83%) and  $\tau_2 = 157 \mu s$  (17%). Possibly, this is caused by hydrogen bonding between the bromide ions and the 2-thenoyltrifluoroacetone ligands, leading to more vibrational deactivation pathways for the excited states. The luminescence spectra of the other homogeneous mixtures were found to be very similar to that of the 99:1 mixture.

## Conclusions

To further explore the mesomorphism of pyrrolidinium ionic liquid crystals, and as an attempt to produce high coordination number ionic metallomesogens (tetrakis(2-thenoyltrifluoroaceto-nato)europate(III) complexes), pyrrolidinium ionic liquid crystals with pendant calamitic mesogenic groups were synthesized. Unfortunately, the europium-containing salts described in this paper were not liquid-crystalline. We assume that the tetrakis ( $\beta$ -diketonato)europate(III) anion is too bulky to be efficiently counterbalanced by the mesogenic units that were used. However, by mixing the europium-containing salts with their bromide analogues, luminescent liquid-crystalline mixtures could be obtained. Many of the other pyrrolidinium salts described in this work showed a rich mesomorphism: not only SmA, SmC, and SmF/SmI phases but also highly ordered smectic phases were observed. The mesomorphism of these compounds depends on the type of anion, the lengths of the flexible alkyl spacer and terminal alkyl chain, and the type of mesogenic group. While the bromide salts showed disordered (SmA and SmC) as well as ordered (E and G, J, H, or K) smectic phases, no highly ordered phases were observed for the bis(trifluoromethylsulfonyl) imide and tetrabromouranyl salts. This was surprising, because the previously described pyrrolidinium tetrabromouranyl salts with long alkyl chains exhibited ordered E phases.<sup>5</sup> The SmA phases were shown to be of the de Vries type. Moreover, we demonstrated that by attaching mesogenic groups, it is possible to induce tilted (disordered and ordered) smectic phases, which are not commonly observed for ionic liquid crystals. Mesomorphic tetrahalometallate salts carrying mesogenic groups and showing tilted smectic phases have not been reported yet. It was not possible to determine general influences of the type of mesogenic group and the length of the alkyl spacer and terminal alkyl chain on the thermal behavior of all the pyrrolidinium ionic liquid crystals. Only conclusions limited to a specific series of salts could be drawn. Because subtle differences in the composition of the cations can have a large influence on the phase behavior, it is not possible to predict which phases will be formed by a certain salt.

**Acknowledgment.** K.G. is a Research Assistant of the FWO-Flanders (Belgium). T.C. is a postdoctoral fellow of the FWO-Flanders. Financial support by the K.U.Leuven (Projects GOA 08/03 and IDO/05/005) and by the FWO-Flanders (Project G.0508.07) is gratefully acknowledged. The authors thank the staff of the Swiss-Norwegian Beamline (SNBL) at the European Synchrotron Radiation Facility (ESRF) (Grenoble, France) for their support with the synchrotron experiments. COSY NMR spectra were recorded by Karel Duerinckx. CHN elemental analyses were performed by Dirk Henot. Mass spectra were measured by Bert Demarsin. TG traces were recorded by Dimitri Soccil. Powder X-ray diffractograms were recorded by Dr. Jan D'Haen and Bart Ruttens (UHasselt, Institute for Materials Research).

(62) Bravo-Grimaldo, E.; Navarro-Rodríguez, D.; Skoulios, A.; Guillon, D. *Liq. Cryst.* **1996**, *20*, 393–398.

(63) Chovino, C.; Frère, Y.; Guillon, D.; Gramain, P. *J. Polym. Sci., Part A: Polym. Chem.* **1997**, *35*, 2569–2577.

(64) Bazuin, C. G.; Guillon, D.; Skoulios, A.; Zana, R. *J. Phys. (Paris)* **1986**, *47*, 927–930.

**Supporting Information Available:** Synthesis and characterization of the precursors and the pyrrolidinium compounds; packing in the crystal structure of compound **6d**, plotted for a  $2 \times 2 \times 2$  supercell, and CIF file of the crystal structure; stack column graphs showing the evolution of the transition temperatures in the series **2a-9a**, **2b-9b**, and **2d-9d**; representative DSC traces and thermograms; additional polarizing optical microscopy textures; table with all Bragg reflections collected from the powder

X-ray diffractograms; evolution of the layer thickness,  $d$ , of the SmA phases shown by selected compounds as a function of the temperature; evolution of the layer thickness,  $d$ , of the different mesophases shown by **7a** and **9d** as a function of the temperature; hypothetical structural model for the SmA phase exhibited by compound **3a**, discarded because of an inefficient space-filling. This material is available free of charge via the Internet at <http://pubs.acs.org>.